12-2019

Preparation of Folic Acid-Carbon Dots-Doxorubicin Nanoparticles as Targeting Tumor Theranostics

Samson Dada
East Tennessee State University

Preparation of Folic Acid-Carbon Dots-Doxorubicin Nanoparticles as Targeting Tumor Theranostics

---

A thesis

presented to

the faculty of the Department of Chemistry

East Tennessee State University

In partial fulfillment

of the requirements for the degree

Master of Science in Chemistry

---

by

Samson N. Dada

December 2019

Dr. Hua Mei, Ph.D., Chair

Dr. Cassandra Eagle, Ph.D.

Dr. Catherine McCusker, Ph.D.

Keywords: carbon dots, nanoparticles, theranostics, chemotherapeutic, doxorubicin.

ABSTRACT

Preparation of Folic Acid-Carbon Dots-Doxorubicin Nanoparticles as Targeting Tumor Theranostics

by

Samson N. Dada

Carbon dots (CDs) have attracted much attention as an excellent gene/drug delivery and biological imaging agent for early cancer theranostics. In this study, we prepared two series of nanoparticles (NPs), which are composed of (CDs) with a targeting agent, folic acid (FA), and a chemotherapeutic agent Doxorubicin (Dox). All the NPs and their intermediates were characterized using ultraviolet-visible spectroscopy (UV-vis), fluorescence spectroscopy, and Fourier transform-infrared spectroscopy (FT-IR). The drug loading capacity (DLC) and drug loading efficiency (DLE) of two series of FA-CDs-Dox were assessed using UV-vis absorption spectroscopy at the wavelength of 485 nm. Both showed good DLE and DLC results when compared to literature data. In addition, the cumulative release property of Dox from the FA-CDs-Dox complexes were investigated in a pH solution of 7.4.

TABLE OF CONTENTS

LIST OF TABLES

Table Page

LIST OF SCHEMES

Scheme Page

LIST OF FIGURES

Figure Page

LIST OF ABBREVIATIONS

CDs	Carbon Dots
QDs	Quantum Dots
FA	Folic Acid
Dox	Doxorubicin
NPs	Nanoparticles
CBNs	Carbon-based nanomaterials
CNT	Carbon nanotubes
UV-vis	Ultraviolet-Visible spectroscopy
FTIR	Fourier transform-infrared spectroscopy
FL	Fluorescence spectroscopy
DLC	Drug load content
DLE	Drug load efficiency
WHO	World Health Organization
HIV	Human Immunodeficiency Virus
AIDS	Acquired immunodeficiency syndrome
DNA	Deoxyribonucleic Acid
RNA	Ribonucleic Acid

Fig	Figure
FDA	Food and Drug Administration
PTT	Photothermal therapy
PEG	Polyethylene glycol
FR	Folate receptors
PEI	Polyethyleneimine
MRI	Magnetic resonance imaging
PBS	Phosphate Buffered Saline
EDC	3-(3-Dimethylaminopropyl)-1-ethyl-carbodiimide
NHS	N-Hydroxy succinimide
MWCO	Molecular weight cut-off
CDR	Cumulative drug release

CHAPTER 1. INTRODUCTION

Cancer is a leading global health concern. It is estimated that about 8.8 million people die of cancer each year, which equates to one out of every six death worldwide, this number far exceeds the total number of deaths from tuberculosis, malaria and HIV/AIDS combined.[1] Our research target is to synthesize water-soluble, bio-absorbable nanoparticles (NPs) that will improve both diagnostic and therapeutic efficacy for cancer. Such theranostic NPs are composed of carbon dots (CDs) conjugated with a targeting agent, folic acid (FA), and an anticancer drug Doxorubicin (Dox).

Statement of Problems

At the time of this writing, reports from the World Health Organization (WHO) show that cancer prevalence has risen to 18.1 million new cases with one in five men and one out of six women globally estimated to develop cancer during their lifetime.[2] It is however surprising that despite the cancer management treatment techniques such as, radiotherapy, chemotherapy, and hormone therapy available, the overall survival rate from cancer has not improved substantially over the past three decades.[3,4]

Similar to many other deadly diseases, studies have shown that the best way to survive cancer is early detection – a stage of cancer characterized by low cellular heterogeneity and metastasis.[5] Oftentimes, detecting early-stage cancer is an onerous task, because during this phase, there are low concentrations of cancerous cells and biomarkers present at the tumor site and in the bodily fluids.[5, 6] Also, since most cancers are detected at the advanced stage, it has been difficult to describe the properties of early-stage tumors, which can be different from advanced-stage cancers. As more cancer cells presented in the late stage, there are more

significant changes in the epigenome, genome, proteome, and transcriptome. These challenges and much more can be solved using nanotechnology driven diagnostics as part of the *nanomedicine* field.[5] For its part, this field provide novel strategies and innovations for early diagnosis and treatment of cancer. It offers competences to perform medical and diagnostics applications unattainable by other strategies.

One challenge to improve cancer treatment outcome lies in personalized therapy that requires real-time feedback on the pharmacokinetics, target site localization, and the healthy organ accumulation of cancer drugs.[7] Compared to other NPs, CDs have recently generated a great deal of attention due to their environmental safety, low-cost, and simple synthesis, functionalization and their potential application as a drug delivery vehicle. To facilitate their clinical transition, however, functionalized CDs require more exploration with regards to scale-up of their biogenic synthesis. Also, since the majority of anticancer drugs are hydrophobic, they can be loaded into the hydrophilic NPs via physical adsorption. But such a method is not very reproducible due to the variance of the amount of the loaded drugs each time. This study will focus on the use of a novel strategy to overcome this limitation by covalently attaching anticancer drugs to FA-CDs complex. As a unique nanodevice, this NPs conjugate has multiple clinical applications for personalized diagnostics and therapeutic cancer treatment.

Cancer Treatment

There are various kinds of cancer treatment based on the type and stage of cancer. Some patients will receive only one type of treatment, while others might require a combination of more than one treatment type, such as surgery with chemotherapy or radiation therapy. Some other types of cancer treatment therapy are immunotherapy, targeted therapy, and hormone therapy.

Of the different types of cancer treatment earlier mentioned, chemotherapy is one of the prevailing treatment techniques used.[8] It involves using drugs to attack and kill cancerous tumors. The chemicals work by stopping and abating the spread of malignant neoplasm. Usually, the drug contains chemicals that damage the DNA or RNA of a cancer cell by interfering with the process of their cell mitosis and meiosis. A regimen, which is a combination of two or three drugs are usually administered to the patients through oral means, via an injection, intravenously, intrathecal, and sometimes topically as determined by the oncologist. The regimen usually can be administered during the early stages of cancer to lower the chances of the cancer relapsing or at an advanced stage to shrink tumor cells and alleviate symptoms.[9] Unfortunately, most cancer drugs are indiscriminate and non-specific, as they kill both cancerous and healthy cells, which often leads consequential side-effects.[8–10] Anemia, diarrhea, and hair loss are common adverse effects experienced when healthy red blood cells, mucous membranes, and hair follicles are affected by chemotherapeutic drugs.[15] According to the National Cancer Institute, there are over sixty-eight drugs widely used in breast cancer treatment as approved by the Food and Drug Administration (FDA).[6]

There are different classifications of anticancer drugs. Figure 1 shows the various kinds of classification of anticancer drugs. The typical chemotherapy drugs are alkylators, antibiotics, antimetabolites, topoisomerases inhibitors, and mitosis inhibitors. Drugs that act on cells are called cytotoxic drugs; an example of these are alkylating agents such as Cisplatin, Carboplatin and Oxaliplatin all of three which have a platinum coordination. Drugs such as Doxorubicin and Dactinomycin are antibiotics and are frequently used in treatment of acute myelogenous and lymphoblastic leukemia, neuroblastoma, Hodgkin and non-Hodgkin's lymphoma.[11]

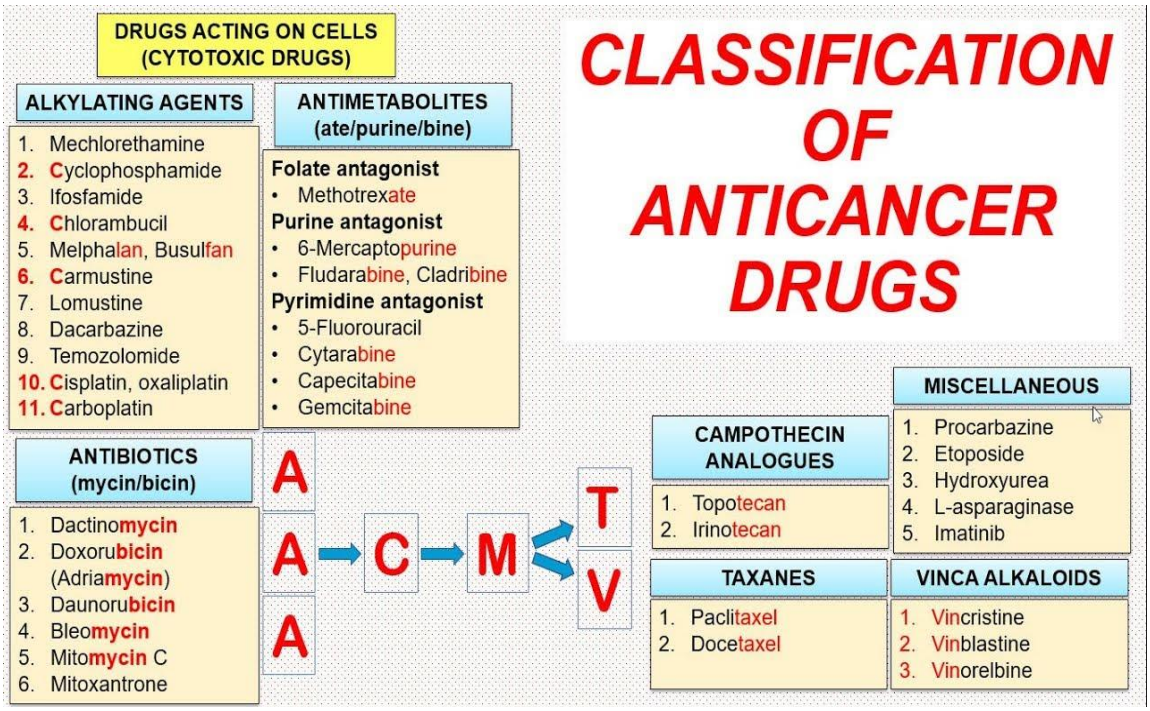

Figure 1. Common classification of anticancer drugs.[12]

Cancer Early Detection

Studies have proven that successful treatment of cancer depends on early diagnosis and detection. Two major factors that contribute to detecting early-stage cancer are screening and giving guidance to the public about the importance of early diagnosis. For example, the public should be aware of early warning signs of cancer, such as irregular bleeding, lumps, and wounds that will not heal. They should be informed on what they should do if they found out they had cancer. Screening is also an effective technique for early cancer detection. It involves conducting various tests on healthy people that show no physical symptoms of the disease. For cervical and breast cancer, mammography and cytological screening are very effective and common methods for early detection of cancer in a mass population.

Theranostic NPs for cancer

Theranostics is a term used to describe the medicines that involve the targeted therapies for various diseases based on specific diagnostic tests.[13] Nanotechnology offers many benefits to develop NPs that would have both therapeutic and imaging functions for early to late-stage cancer detection and treatment. Over the last decade, nanoparticles made of carbon-based materials continue to draw attention in theranostic studies due to their capability to act as a drug delivery vehicle. Simple prototypes are designed for cancer studies and research, where carbon NPs are conjugated to a specific anticancer drug that is active towards an overexpressed receptor for bioimaging and drug delivery functions.[14] Since studies have shown that amorphous carbon NPs emit in the visible region on surface modification which may be utilized in *vivo* imaging applications.[15]

Carbon based nanomaterials, such as buckminsterfullerene (e.g., C_{60}), carbon nanotubes (CNTs), graphene, quantum dots (QDs), and nanodiamonds, have drawn a large interest as potential drug delivery vehicles and imaging materials due to their special luminescence properties. For examples, light sources in the UV, visible and infrared region, which ranges from 200 – 1000 nm can be employed in carbon-based NPs light-activated drug delivery therapies. Studies have reported that photothermal therapy (PTT), which involves the special NPs converting the light energy into heat to attack tumor cells through a process called photoablation.[16,17] The use of carbon based NPs to carry the anti-cancer drugs into cancerous cell nuclei by pH-controlled endocytosis has also been reported.[10] Figure 2 below shows the biomedical applications of these carbon nanomaterials in bioimaging and cancer therapeutic studies.[17]

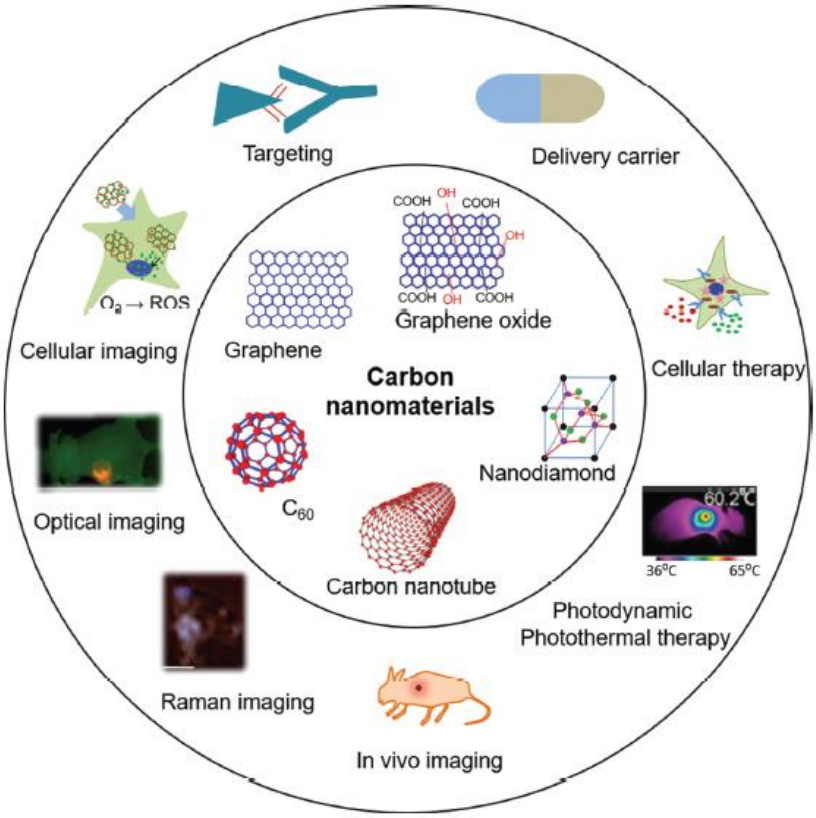

Figure 2. Carbon-based nanomaterials (CBNs) and their diverse applications in theranostics.[17]

Quantum Dots (QDs)

Inorganic QDs have been widely studied as a bioimaging and optical sensing agent due to their high quantum yield, chemical stability, and excellent photoluminescence behaviors. Before the development of CDs, inorganic QDs were first discovered for disease diagnosis and screening. The QDs' confocal, multiphoton, and electron microscopic imaging have resolutions better than 10 nm. They were synthesized from heavy metals such as cadmium, tellurium, and selenium. Their core and shell usually are composed of semiconductors from inorganic compounds, such as CdS/ZnS, CdSe/ZnS. [18–22] Due to their size advantage, they were initially used in cancer immunotherapy for tracking molecules.[23]

Consequently, application of QDs in genetic disease diagnosis and screening have been reported.[24] QDs have been widely used *in vivo* studies of small animals such as mice because they have better stability and quantum yield compared to organic fluorophores that absorb in the IR region.[23] For instance, as shown in Figure 3, the application of QDs in the imaging of embryonic stem cells used one single excitation wavelength. This study reveals that semiconductor QDs can be applied in both *in vivo* and *in vitro* cellular imaging. The applications of QDs as biological imaging agents and drug carriers are also widely investigated.[25] Unfortunately, even though QDs have luminescent properties that are sometimes twenty times brighter and hundred times more stable than most fluorescent materials, studies have shown QDs can bind to certain thiol groups in the mitochondria of a cell causing cell apoptosis, which has prevented their use in clinical applications.[23,26,27]

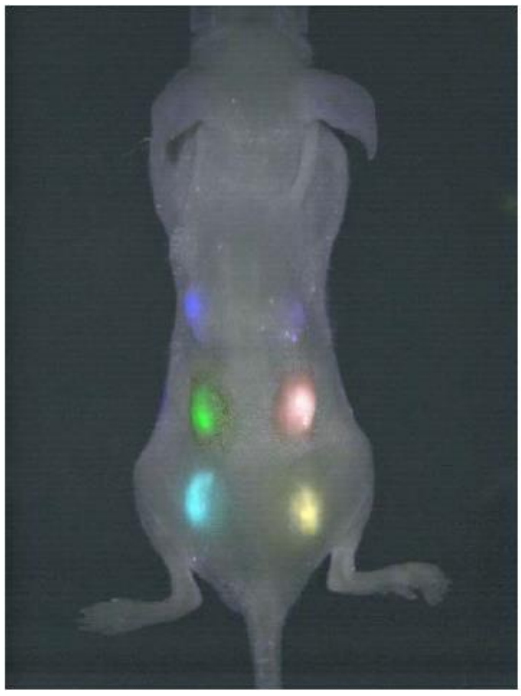

Figure 3. Embryonic stem cells labeled with six different QDs were subcutaneously injected on the back of the athymic nude mice right after labeling (image taken with a single excitation light source right after injection.[28]

Carbon Dots (CDs)

During the last ten years, CDs have garnered more interest due to their unique properties and are frequently reported as better substitutes to inorganic quantum dots (QDs). CDs are generally classified as a group of quasi-spherical carbon NPs with sizes not more than 10 nm.[10,29,30] Studies have shown that CDs are primarily of interest in biological applications due to their unique properties such as fluorescence, extremely high biological compatibility, and superficial synthetic route.[31–33] Different sample preparation methods have been reported for these "nanolanterns" since their discovery. Generally, those methods are classified into two strategies; the "bottom-up" approach and the "top-down" approach. The top-down approach usually involves the breaking down of large carbon material under very harsh conditions. Some examples of this method includes oxidative acid treatment, arc-discharge, laser ablation, and electrochemical exfoliation.[11, 29, 32–35]

While the bottom-up approach, on the other hand, involves synthesis from small carbon containing precursors and chemicals that contain functional groups such acids, amines, and hydroxyl groups. [31] Some example of the bottom-up technique include; microwave, ultrasonic, hydrothermal, and acid treatment.[30] Table 1 summarized the methods mostly used in preparation of CDs.

Table 1. Strategies employed in CDs synthesis.[28, 36]

Top Down Synthesis	**Bottom-up Synthesis**
Arc discharge	Hydrothermal treatment
Electrochemical exfoliation	Ultrasonic
Laser ablation	Microwave
Oxidative acid treatment	Thermal combustion

Each synthetic method mentioned in Table 1 has its advantages and disadvantages, some of which are outlined in Table 2 shown below. For example, chemical ablation is very much accessible but is usually done under a very harsh condition, involving multiple steps leading to a poor control over sizes. In this study, two series of CDs were prepared using the hydrothermal method, which is by far the most favorable, and the most commonly used technique for CDs synthesis. The reason for this is that the technique is generally cost effective, eco-friendly, and non-toxic.[31,39]

Table 2. Advantages and disadvantages of common synthetic methods of CDs.[39]

Synthetic Methods	Advantages	Disadvantages
Chemical ablation	Most accessible, various sources	Harsh conditions, drastic processes, multiple-steps, poor control over sizes
Electrochemical carbonization	Size and nanostructure are controllable, stable, one-step	Few small molecule precursors
Laser ablation	Rapid, effective, surface states tunable	Low QY, poor control over sizes, modification is needed
Microwave irradiation	Rapid, scalable, cost effective, eco-friendly	Poor control over sizes
Hydrothermal/solvothermal treatment	Cost effective, eco-friendly, non-toxic	Poor control over sizes

Furthermore, the optical properties of CDs are highly related to the reaction method, starting reactants, size of the particle, structure, and surface state, and therefore, can be regulated. CDs are known to exhibit an excitation-dependent wavelength, which has made it useful in multi-color imaging applications. It is essential to keep in mind that the optical behavior of CDs

fluctuate and are inconsistent for different starting material and synthetic methods used. The mechanism for this behavior is puzzling, and the reason is largely unknown.

Nonetheless, since future perspective of CDs focuses on clinical applications, the cytotoxicity of CDs, as well as their compatibility with living organisms, are being investigated. So far, biological *in vivo* studies carried out in mice and zebra fish showed that CDs have no apparent lethal effects. It is why CDs are preferable materials in biological application and *in vivo* studies in comparison to inorganic QDs.[40–42]

Applications of CDs

CDs have been employed in a wide range of applications such as drug delivery,[30,43,44] biological imaging,[45–48] light emitting devices,[49] and photo-catalysts. [50–53] Several studies continue to explore the potential application of CDs. Figure 4 below shows some common applications of CDs.

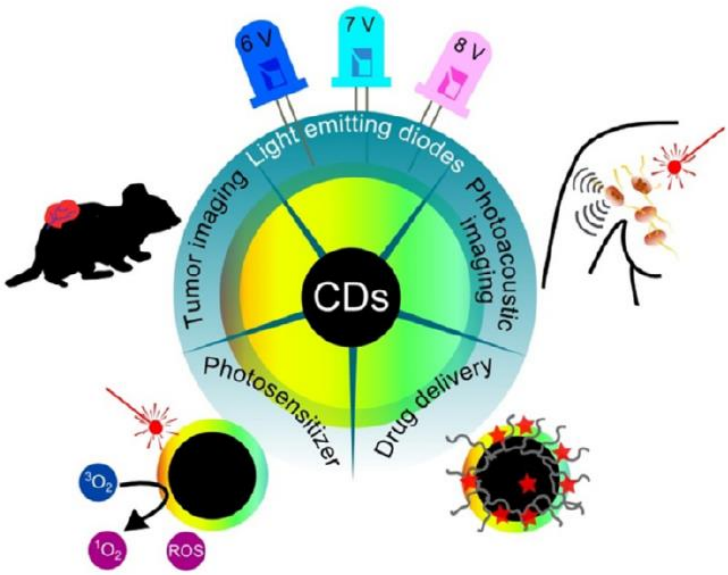

Figure 4. Some common applications of CDs.[54]

Biological Imaging Applications

One of the most commonly used application of CDs is in target-specific imaging applications. CD imaging have been widely explored in biological imaging of different types of organism and prokaryotes, such as bacteria, eukaryotes, and fungi. Sheng-Tao Yang and his group were the first to report the practical application of CDs in *in vivo* studies in 2009.[40] Polyethylene glycol-functionalized CDs were injected subdermal and intravenously into a lab mice. It was observed, as in the case of the subdermal injection, that the area injected exhibited a substantially high fluorescence but faded away in 24 hours post-injection. However, when the intravenous injection was carried out, only the bladder region showed fluorescence, 3 hours after this, CDs were found in the urine. Further *ex vivo* studies showed the accumulation of CDs on the kidney but not on the liver. This study showed that CDs can be removed from the body when injected intravenously.[55]The conditions for using CDs for biological imaging and diagnostic studies are challenging. The parameters, such as cytotoxicity, cellular uptake, hemocompatibility, and quick excretion from the body, need to be examined.[56]

Drug Delivery Systems

Drug delivery is a technique used for systematic target delivery and control of curative agents. Studies have shown that the surface of CDs can be modified for gene transfer and drug delivery functions. For instance, Liu et al. used polyethyleneimine (PEI) modified CDs for gene transfer and bioimaging studies.[57] The study proved that CDs had both transfer ability and excellent fluorescence property that helped provide useful data for studies on plasmid DNA physiological conditions. It was noted that during the transfer process, CDs maintained their unique excitation-dependent fluorescence. Also, CDs modified with polyethylene glycol (PEG)

have also been conjugated with Dox to improve the specificity of Dox for cancer cells.[58,59] Figure 5 below shows applications of CDs loaded with Dox for targeting specific cancer cells.

Carbon Nanoparticles	Drug Loaded	Ligand Attached	Cell Targeted
C-dots	Dox	Nuclear localization signal peptide	A549
C-dots	Dox	-	HeLa
C-dots	Dox	-	HeLa
C-dots	Dox	Transferrin	CHLA-266, SJGBM2
C-dots	Dox	Folic acid	HeLa
C-dots	-	Folic acid	HeLa, NIH-3T3, MCF-7
C-dots	-	Folic acid	HepG-2
C-dots	Gene	Hyaluronan	HeLa

Figure 5. Some examples of CDs application in drug delivery systems.[14]

Sensing

The unique properties and fluorescence behavior of CDs have made them useful materials for detecting a wide range of analytes, cations, micro and macromolecules, cells, and bacteria.[60] Over the past decade, studies started to focus on fluorescence (FL) based sensing, due to their unique properties such as outstanding sensitivity, relatively quick response time, and affordability. In the early 2000's fluorescent sensory materials such as organic dyes, quantum dots, fluorescent proteins, etc. have been developed. Even though the practical use of some of these materials have been reported, they often have worrisome disadvantages that have caused limitation of use. The surface of CDs, on the other hand, has been used for detection of mercury cations and thiols as reported by Lu et al.[61]. This unique ability to modify the surface of CDs has made them superior to many other materials used as biosensors. For instance, CDs obtained from using glucose as a precursor exhibited a high affinity for boric acid due to the hydroxyl groups on the CDs surface such CDs have been applied in the detection of glycoproteins.[62]

Research Design

The primary goal of this study is to prepare novel CDs based nanoparticles as potential theranostic for cancer treatment. The designed NPs (Figure 4) consist of three main components CDs, the targeting agent folic acid (FA), and the antic-cancer drug Doxorubicin (Dox), as illustrated in Figure 6. The research designs are summarized as following;

1. To synthesize two series of CDs using the hydrothermal bottom-up approach.
    a. To change the ratio of the starting materials, two kinds of CDs will be prepared with different functionalities on the surface.
    b. To characterize CDs using UV-vis spectroscopy, fluorescence spectroscopy, and infrared spectroscopy.
2. To prepare FA-CDs by conjugation of CDs to FA using a non-cleavable peptide bond linker.
    a. To characterize FA-CDs using UV-vis spectroscopy, fluorescence spectroscopy, and infrared spectroscopy

3.To load anticancer drug Dox onto FA-CDs, via a pH cleavable bond.

    b. To characterize FA-CDs-Dox properties using UV-vis spectroscopy, fluorescence spectroscopy, and infrared spectroscopy

a. To analyze the drug load content (DLC) and drug load efficiency (DLE) properties of FA-CDs-Dox

b. To investigate the drug release at different pH and compare data of the two series prepared.

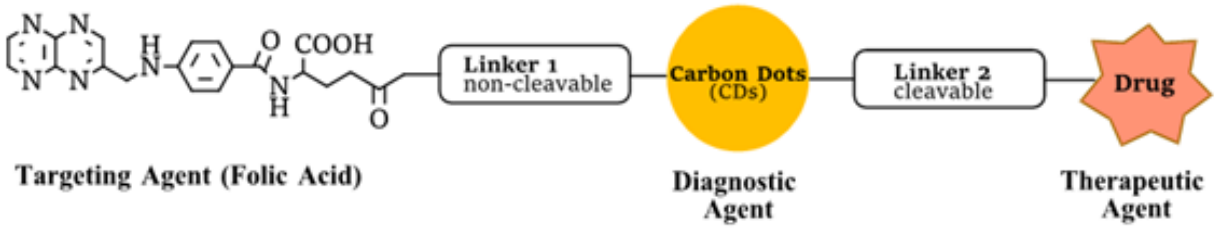

Figure 6. Structural design of FA-CDs-Dox cancer theranostics.

Research Plan

Two series of CDs will be first prepared using the hydrothermal technique by heating different ratio of citric acid, and ethylenediamine at 250 °C.[63] The precursors were strategically chosen as they can provide the –COOH, $–NH_2$ and –OH functional groups for further modification. In order to improve the target specificity to the tumor cells, the CDs are permanently linked to FA via an amide bond. Furthermore, the FA-CDs NPs are used to facilitate the delivery of the anticancer drugs Dox through a pH-cleavable linker (electrostatic attraction).

Folic Acid (FA)

Folic acid is a water-soluble, low molecular weight vitamin that plays an essential role in cell survival and has high affinity to the folate receptors (FR). Three isoforms of the FR have been identified (FRα, FRβ, and FRγ), the α type is the most common subtype of FA transport. Different kinds of tumors, such breast, ovarian, pancreatic, lung, head and neck, prostate, ovarian cancers, and mesothelioma, overexpress of this FR.[64,65] Generally, FR are glycosylphosphatidylinositol anchored cell receptors that are highly expressed in various types of cancer. Interestingly, this type of cell receptor is not present in healthy cells.[66] Several studies have reported the use of FA (as shown in Figure 7) in cancer studies.[67–72] This is because FA can be easily conjugated to theranostic agents for targeted deliveries, also, its high affinity to the

folate receptor is sustained even after conjugation to the diagnostic and therapeutic agent (K_d = 10^{-10} M).[73,74] Furthermore, studies have proven that FA consumption does not increase the risk of getting any form of cancer.[75] Several drugs, ligands, and curative agents have linked to FA for tumor selective drug delivery. Some examples are protein toxins, chemotherapeutic drugs, oligonucleotides, radio-imaging agents, gene therapy vectors, and magnetic resonance imaging (MRI) contrast agents.[73]

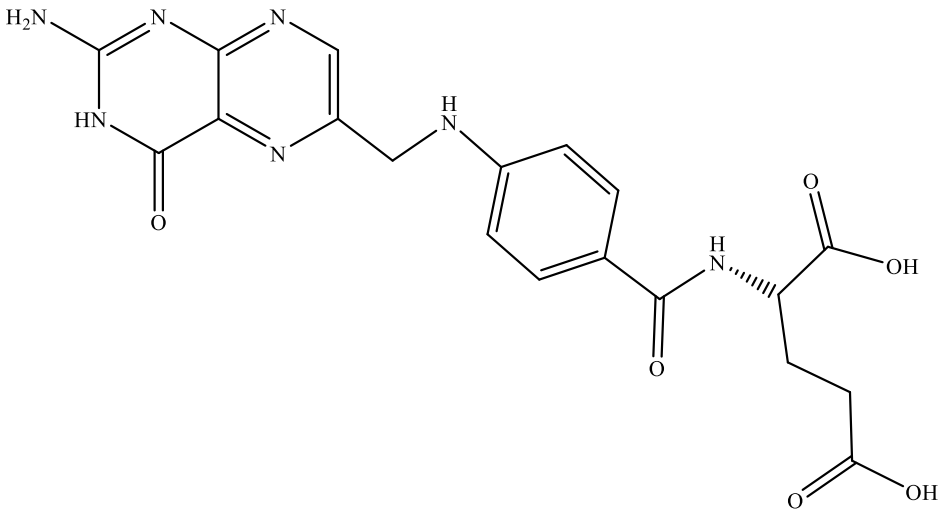

Figure 7. The chemical structure of folic acid

Dox

In the early 1950s, there was incessant search for anticancer compounds from soil-based bacteria such as the *Streptomyces spp.* Not too long after that, a new strain of the bacteria was isolated that produced an antibiotic that showed potency against mouse tumors. The new compound, which was named daunoribicin. However, it has serious side effect, such as cardiac toxicity. And then, scientists made genetic modification to the bacterium form Adriamycin. The Dox (Figure 8) was finally made to mitigate some series side effect.[76] Dox is a potent, low-cost

chemotherapeutic drug, which belongs to the class of anthracyclines. Even though the full mechanism of action of Dox is not fully understood, Dox are known to interfere with the process of cell replication and transcription by DNA double-helix intercalation, mitochondrial dysfunction, and sometimes by oxidative stress by production of a reactive oxygen species (ROS).[10,11,77,78]

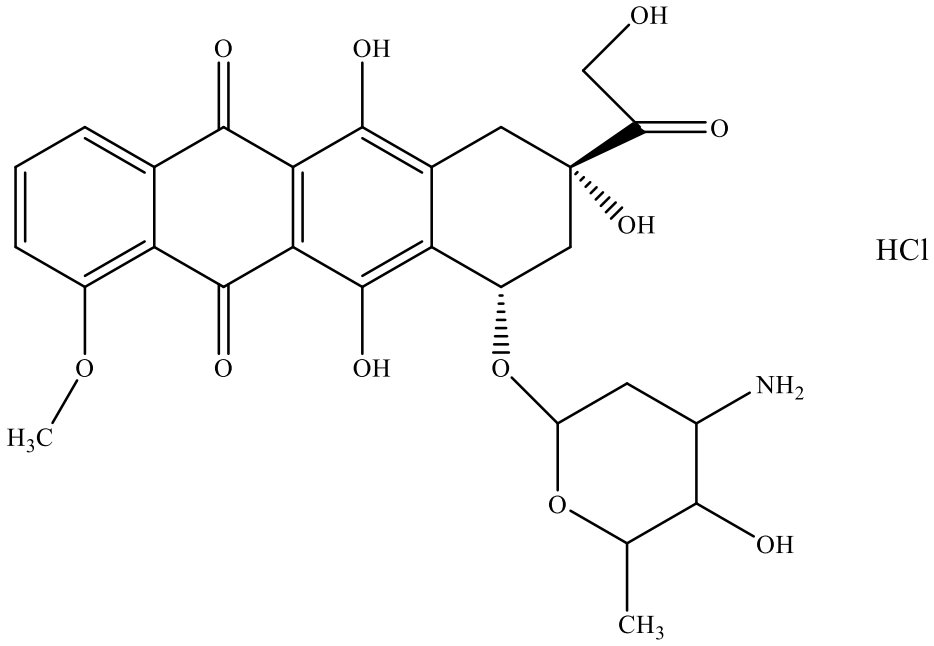

Figure 8. The chemical structure of Doxorubicin • Hydrochloride

Unfortunately, similar to most other traditional anticancer drugs, Dox is indiscriminate and is also non-specific, which means that it attacks both cancerous and healthy cells. Some side effects, such as cardiomyopathy, have also been reported.[79] The adverse effects and the non-specific distribution of traditional chemotherapeutic drugs is one of the greatest challenges troubling cancer chemtherapy.[8] Dox which is an amphipathic base has a pK_a value around 8.3 and in an environment of a pH of 7.4, it exists as a cation due to protonation of its amino functional group.[80] This phenomenon has its advantage because Dox can be potentially loaded on the negatively charged carbon nanoparticles via electrostatic interaction and π-π stacking.[14,30,81]

This unique interaction has many times been utilized to deliver Dox to cancerous cell nucleus via a pH-controlled release system. Another mode of delivery of Dox that has been reported is via the formation of an amide bond or a Schiff base, and this is formed by reacting the amino group of Dox with the carboxylic acid functional group of the carbon NPs.[82,83]

Fundamental Spectroscopic Techniques

To study the photoluminescence of CDs and its based NPs, it is important to understand the theories behind optical spectroscopies such as absorption, fluorescence, and infrared spectroscopy. Figure 9 below shows different types of technique and their corresponding wavelength region.

Wavelength Region	*Wavelength Limits*	*Type of Spectroscopy*	*Usual Wavelength Range*	*Types of Transitions in Chemical Systems with Similar Energies*
Gamma rays	0.01–1 Å	Emission	<0.1 Å	Nuclear proton/neutron arrangements
X-rays	0.1–10 nm	Absorption, emission, fluorescence, and diffraction	0.1–100 Å	Inner-shell electrons
Ultraviolet	10–380 nm	Absorption, emission, and fluorescence	180–380 nm	Outer-shell electrons in atoms, bonding electrons in molecules
Visible	380–750 nm	Absorption, emission, and fluorescence	380–750 nm	Same as ultraviolet
Infrared	0.075–1000 μm	Absorption	0.78–300 μm	Vibrational position of atoms in molecular bonds
Microwave	0.1–100 cm	Absorption	0.75–3.75 mm	Rotational position in molecules
		Electron spin resonance	3 cm	Orientation of unpaired electrons in an applied magnetic field
Radiowave	1–1000 m	Nuclear magnetic resonance	0.6–10 m	Orientation of nuclei in an applied magnetic field

Figure 9. Wavelength Regions, Spectroscopic Methods, and Associated Transitions.[84]

Absorption Spectroscopy

When a sample is continuously exposed to a radiation, some portion of this radiation may be absorbed by the sample, which can be observed on an absorption spectrum.[84,85] The Jablonski diagram, as shown in Figure 8, may be used to represent the discrete and quantized electronic

energy of different molecules. Before being exposed to a radiation, electrons mostly remain at the lowest occupied energy level otherwise known as the ground state. However, when electrons absorb light energy they move to a higher energy, or excited state.

The photon absorbed by the sample is wavelength-dependent and is proportional to the absorbing sample concentration. In practice, the analyte to be studied is placed in a cuvette such that radiation can be allowed to pass through it, the amount of radiation passing through the sample solution is then compared to a reference solution. Molecules on absorption of energy photons typically moves to the lowest unoccupied molecular orbital (LUMO) from a highest occupied molecular orbital (HOMO), It is possible for a compound to exhibit more than one electronic transition as shown in Figure 10.

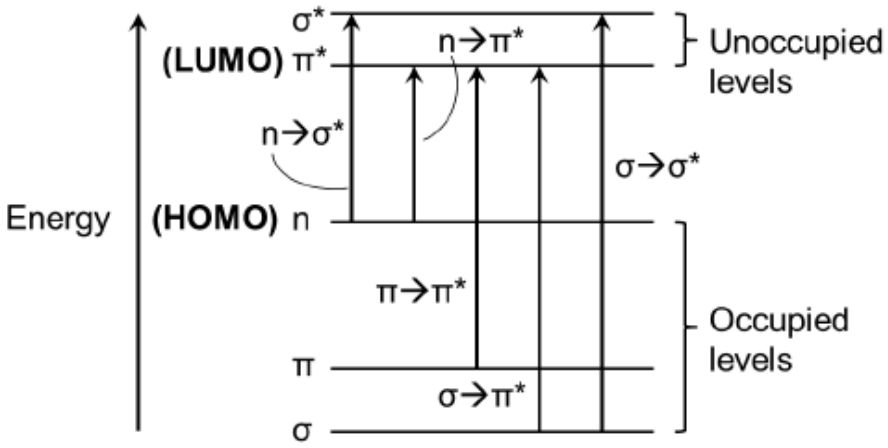

Figure 10. Diagram showing possible electronic transitions.[86]

UV-vis Absorption

UV-vis absorption spectroscopy typically ranges from 200 to 1000 nm. Among them, the UV range is within 200 – 350 nm and the visible range is from 350 – 700 nm [84]. UV-vis absorption spectroscopy is a typical technique to characterize CDs. Different absorption range has been reported for CDs depending on the starting material and the preparation methods. As Zhu et al. reported, two major peaks for the CDs are at 240 and 344 nm from four samples of CDs prepared using the same technique but at different temperatures. Fig. 11 shows the combined UV-vis absorption spectra of these four CDs samples. It is noted that as the temperature increases, the absorption peak at 344 nm (surface/molecule section) decreases while the peak at 240 nm (carbonic core section) increases.[63] This temperature dependent behavior of CDs is frequently reported. The carbogenic core of CDs is known to increase on increase in temperature. To understand the emission behavior of CDs, the fluorescence spectroscopy is often used since the light emitted at the electronic excited state is not reported on a UV-vis spectroscopy.

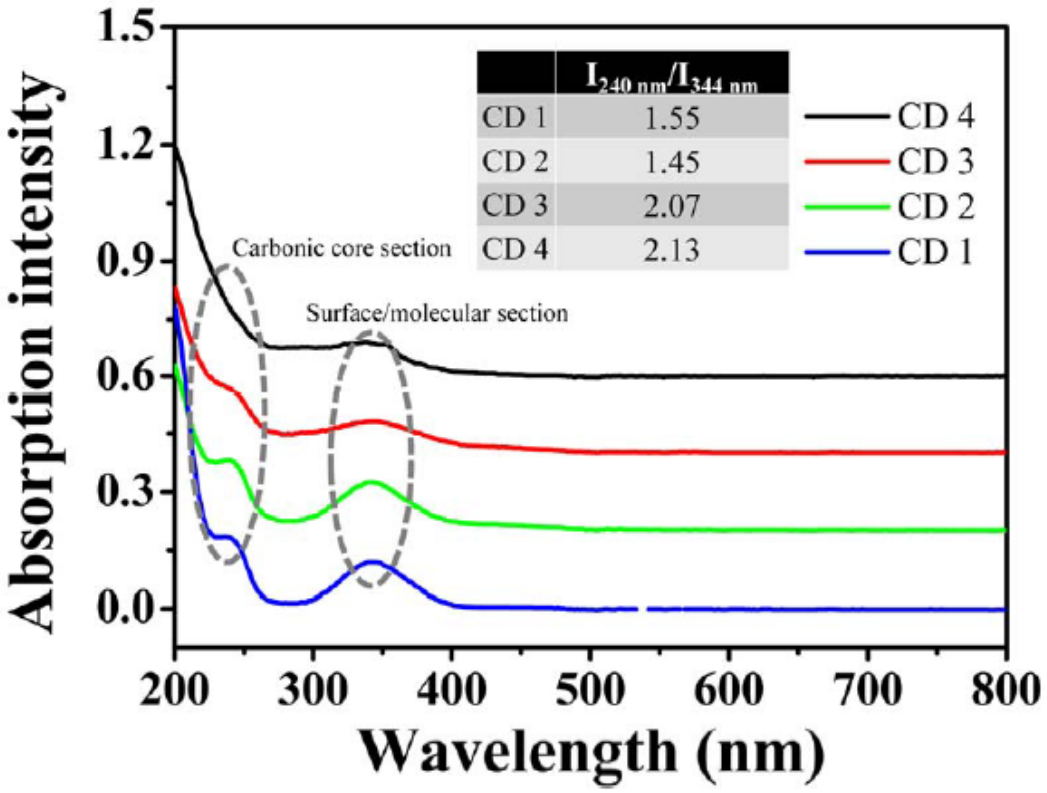

Figure 11. The UV/Vis absorption of CD 1-4.[63]

Fluorescence Spectroscopy (FL)

Another spectroscopic technique to characterize CDs based NPs is fluorescence spectroscopy. In fluorescence spectroscopy, the signal detected is from the radiation emitted from the analyte as it returns to the ground state after excitation. While in phosphorescence emission takes place at the triplet excited states, also more generally, phosphorescence is when the spin of the ground and excited states is different. In both cases, the analyte will first exhibit excitation as a result of absorption of energy radiation in the ultraviolet range before emission.[87] The typical fluorescence spectrum of CDs is dependent on the mode of preparation and the starting material used. In general, CDs exhibit an excitation dependent fluorescence behavior.

The experiments conducted by Zhu et al. show that CDs have an emission maximum wavelength at 443 nm, which explains why it appears blue when viewed under the UV lamp (Figure 12).[31]

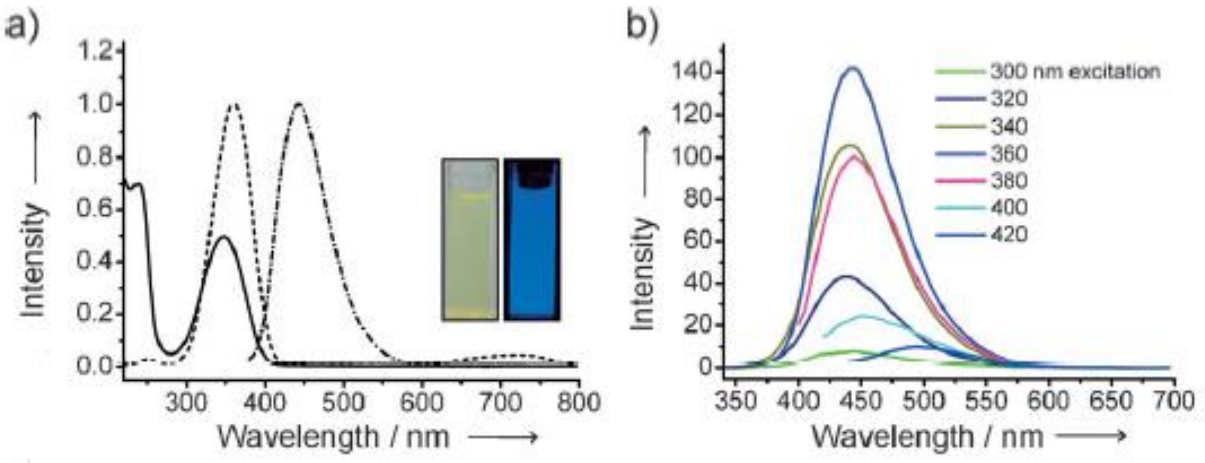

Figure 12. UV/Vis absorption (——), PL excitation (------), and emission (--•--•) spectra of CDs in aqueous solutions. Insets show photographs of CDs in aqueous solution under visible (left) and UV (right) light. b) Excitation-dependent PL of CDs.[31]

Infrared Spectroscopy

The last optical spectroscopic technique we used to characterize the CDs based NPs is Fourier transform infrared spectroscopy (FTIR). Primarily these were used to identify the types of functional groups and bonds present in the samples. The types of bonds present in a molecule can be determined using their bond vibrations relative to the specific frequency of infrared radiation absorb by the molecule. The infrared radiation absorbed by the molecule is usually expressed in wavenumber (cm^{-1}). Generally, infrared spectroscopy ranges from 400 – 4000 cm^{-1} and can be used to identify specific functional group and chemical bonds present in a molecule. Infrared spectroscopy is very much similar to absorption and emission spectroscopy in that the frequency of infrared radiation absorb by a molecule correlates with the nature of the chemical bond present in that molecule. In this study, IR spectroscopy is used to confirm the existence of

certain functional group outshell of the CDs based NPs. The functional groups such as carbonyl, acid, hydroxyl, amide bonds, etc. of NPs, are easily detected by IR.

CHAPTER 2. EXPERIMENTAL

General Consideration

UV-vis Spectroscopy

The UV-vis analysis was done using a double beam UV-vis spectrometer (PharmaSpec UV-1700, PerkinElmer, USA). Various concentrations of the samples and intermediates were prepared in deionized water. The absorption spectra were taken in a one-centimeter path length quartz cuvette using deionized water as the reference material. Typically, the absorption readings were recorded from 800 nm to 190 nm. All the noticeable absorption maxima were noted and were reported.

Fluorimeter

The fluorescence emission spectra measurements were taken in an aqueous solution in air using a fluorimeter (FluoroMax-3, Jobin Yvon Inc, USA) with a slit width set at 10 nm for both excitation and emission monochromators using a Xenon arc lamp. Measurements were taken using a standard 1 cm quartz cuvette. For each sample, were recorded from 400 to 700 nm, the data was not corrected for instrument response. Also, since the samples exhibited an excitation-dependent fluorescence as earlier mentioned, the emission spectra were taken at various excitation wavelengths.

Infrared Spectroscopy

The infrared spectra were recorded with a Shimadzu IRPrestige FTIR. Spectra of the neat powered were recorded using the ATR accessory. The infrared (IR) spectra was collected from

4000 cm^{-1} to 450 cm^{-1}, and the quotation of wavenumbers (cm^{-1}) to intensity abbreviations was strong (s), very strong (vs), and medium (m). Others include weak (w) and very weak (vw).

Materials and Methods

Ethylenediamine, citric acid, Doxorubicin hydrochloride (Dox•HCl), dialysis bag (MWCO = 1000 and 3500 Da), N-Hydroxysuccinimide (NHS), 3-(3-Dimethylaminopropyl)-1-ethyl-carbodiimide (EDC), folic acid, gibco 1X phosphate buffered Saline pH 7.4 were all obtained from Fischer scientific, USA.

Preparation of CDs, FA-CDs and FA-CDs-Dox

Synthesis of CDs

Two series of CDs were prepared as described by Zhu Shoujun and his co-workers with some modifications.[63] The first series of CDs (Sample A) contained 2.000 g (10.41 mmol) of citric acid (CA) mixed with 63.74 µL (0.9540 mmol) of ethylenediamine (EN) (The 9:1 ratio), dissolved in 10.00 mL of deionized water. The second series of CDs (Sample B) contained 1.051 g (5.470 mmol) of citric acid mixed with 335.0 µL (5.014 mmol) of ethylenediamine (1.1:1 ratio), dissolved in 10.00 mL of deionized water. Both samples were transferred into an autoclave to react at 250 ^{o}C for 5 hours. The samples were collected and allowed to cool, after which they were dialyzed in the 3500 Da dialysis bag placed in 500 mL of deionized water for 6 hours. The final samples were collected and lyophilized to obtain the brown-black product.

Synthesis of FA-CDs

Two series of FA-CDs were prepared as the procedure described by Zhao et al.[67] For the typical procedure, firstly, 20 mg of FA was sufficiently dissolved in 8 mL of 1X PBS buffer (pH 7.4) to get a clear yellow solution. Then, 4 mL aqueous solution of 0.0260 g (0.1356 mmol) EDC and 0.0156 g (0.1355 mmol) NHS was added to the solution of FA. The mixture was treated by sonication at room temperature overnight to form the o-acrylisourea intermediate, then mixed with 2 mL of CDs (22 $mgmL^{-1}$). The reaction was maintained under the same conditions for another 24 hours. Next, the solution was dialyzed (using MWCO 1 000 Da) against distilled water for one day to remove the excess FA or CDs. Lyophilization of the resulting product was then carried out to obtain a yellowish powder.

Synthesis of FA-CDs-Dox

Two series of FA-CDs-Dox were prepared as the procedure described by Yuan et al.[8] For the typical procedure, 1 mL of FA-CDs solution (8 mg mL^{-1}) and 1 mL of Dox solution (0.4 mg mL^{-1}) were mixed with 2 mL of PBS at pH 7.4 under stirring to form a final solution system of 4 mL. This solution was then allowed to stir for 24 hours on a sand bath set at 25^{o}C and 200 rpm in the dark. After that, the resultant solution was dialyzed using a dialysis membrane (MWCO = 3,500 Da) against 500 mL deionized water for 2 hours to remove any unreacted Dox or FA-CDs. The reaction was carried out in the dark to prevent photodegradation of Dox. A pink-reddish solid product was obtained after the solution was lyophilized for 48 hours.

Characterization

Spectral properties of all the NP, such as CDs, FA-CDs, and FA-CDs-Dox, were studied by UV-vis spectroscopy, fluorescence spectroscopy (FluoroMax-3, Jobin Yvon Inc, USA) using a standard quartz cuvette having a path length of 1 cm.

The samples were also analyzed by Fourier-transform infrared spectroscopy (FTIR) by an IR Prestige-21 spectrometer (Shimadzu, USA) equipped with a Pike Miracle ATR sampling accessory. The spectra were obtained from the average of 16 scans from 600 to 4000 cm^{-1} at 4 cm^{-1} resolution.

Drug Load Content (DLC) and Drug Load Efficiency (DLE)

DLC and DLE were determined using the method as described by Kong et al. with few modifications.[88] The FA-CDs-Dox aqueous complex was dialyzed against pure water for 8 h and the concentration of unbound drug was measured spectrophotometrically at 485 nm and calculated using the standard calibration curve of Dox (linear line equation =2.27x +0.2229). The DLC and DLC were calculated using the following equations:

$$DLC(mg/g) = \frac{amount\ of\ Dox\ loaded\ in\ FA-CDs}{initial\ amount\ of\ FA-CDs}$$

$$DLE\ (\%) = \frac{amount\ of\ Dox\ loaded\ in\ FA-CDs}{initial\ amount\ of\ the\ Dox}\ x\ 100\%$$

In-vitro Drug Release

The pH dependent release of Dox from FA-CDs-Dox complex was also investigated. For a typical procedure, 3 mL of FA-CDs-Dox aqueous solution was sealed in a dialysis bag (MWCO = 1,000 Da) and in 120 mL PBS solution at pH 5.0 and heated at 37 ^{o}C under mild intermittent

stirring. The samples were collected at intervals of 30 min for 3 h and then at intervals of 24 h for 3 days. At regular intervals, 2 mL of the release medium in PBS was taken and replaced with fresh PBS solution of the same volume. The standard calibration curve was taken at 485 nm and the amount of released Dox was determined. Determination of the concentration of drug released in the mixture was done using the formula y = mx+b, y is absorbance of the unknown, m is slope, b is intercept, x is concentration (mg/mL)[89]. Slope = 22.000, intercept = -0.0467, R^2 = 0.9988. The same procedure was repeated at pH 7.4.[90]

CHAPTER 3. RESULTS AND DISCUSSION

Synthesis of CDs

The synthesis of CDs was done using one pot hydrothermal treatment of citric acid and ethylenediamine.[63] Scheme 1 below shows the reaction scheme. The surface of prepared CDs contains the primary amine and carboxylic acid functional groups which are facile for further modification. The same technique was applied for synthesis of both sample A and B from different ratio of starting materials. A low yield of approximately 33% *Wt.* was obtained for sample A and a yield of 35% wt. was obtained for sample B. The reason for low yields of this step may because some of the products might have been washed off during the dialysis procedure.

It was noted that the lyophilization process of sample B took approximately 48 hours which is relatively shorter compared to sample A, which took over 120 hours. This result also shows that the changing the ratio of citric acid and ethylenediamine can influence the purification process of the product. The sample was stored in the refrigerator and subsequently prepared for characterization.

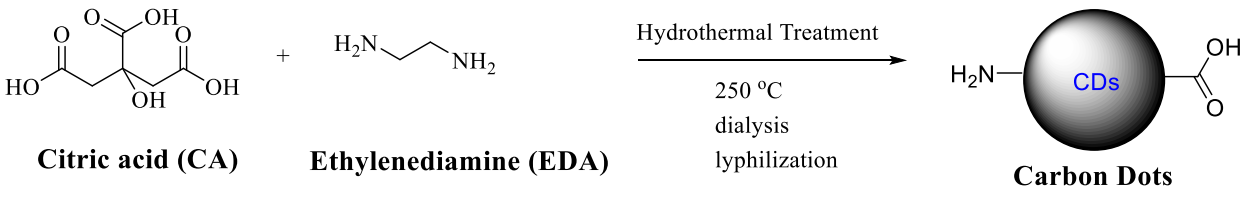

Scheme 1**.** Hydrothermal synthesis of CDs. (The ratio of functional groups, or starting material is not shown).

UV-vis and FL Spectroscopy Result of CDs (Sample A and B)

UV-vis Results (Sample A)

The UV-vis of CDs Sample A (Fig. 13) reveals that the CDs solution (0.1 mg mL^{-1}) showed characteristic absorption peak at 201 nm and 346 nm. Those peaks indicate the presence n-π* and π-π* transitions of the carbonyl group on the surface of the CDs.[83] The results are similar to the data reported from Dr. Shoujun Zhu and his group, in which an aqueous solution of CDs showed a major absorption peak at 344 nm.[63]

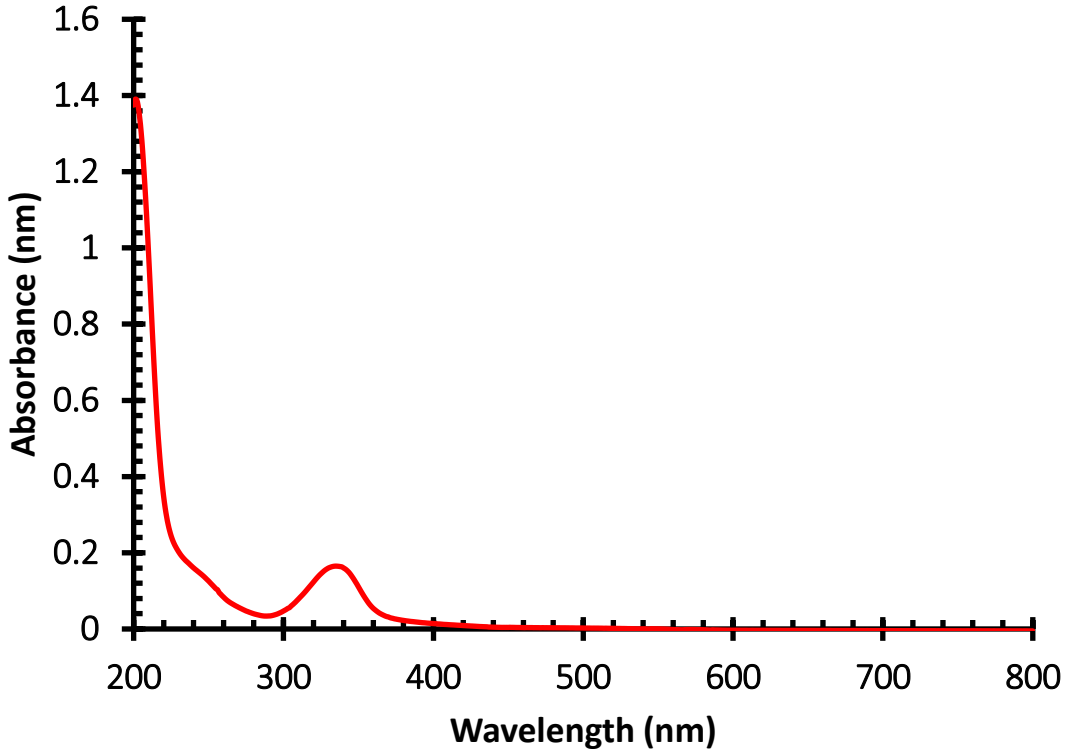

Figure 13. UV-vis of 0.1 mgmL^{-1} aqueous solution of CDs (Sample A)

UV-vis (Sample B)

The UV-vis analysis of CDs sample B (Figure 14) was carried out the same way as sample A for comparison. The CDs solution (0.1 mg mL^{-1}) showed characteristic absorption

peak at 206 nm and 337 nm. The absorption at 337 nm of sample B is much higher than sample A for all concentrations, this may be due to the hyperchromic effect of the N-H functional group close to the carbonyl group. The absorption peaks at 206 nm and 337 nm also reveals the presence of π-π* and n-π* transitions of the carbonyl group on the surface of the CDs. Like sample A, solution of sample B also showed blue luminescence when viewed with a hand-held UV lamp as shown in Figure 15.

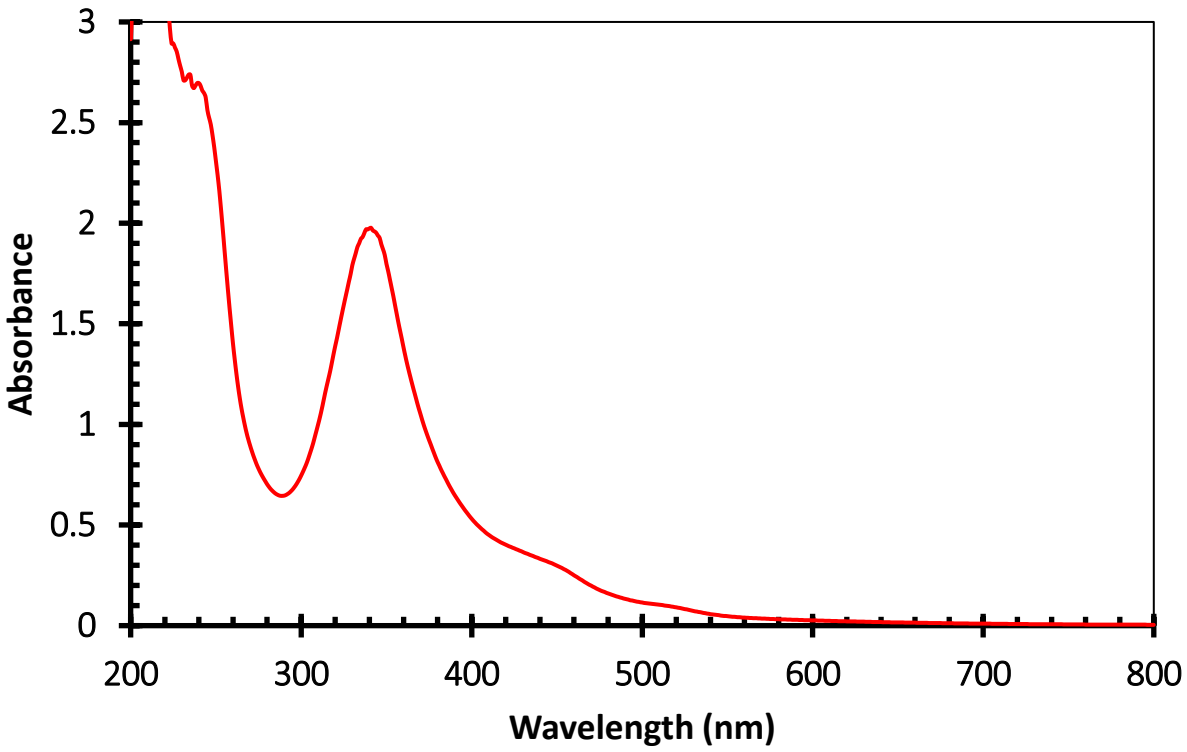

Figure 14. UV-vis of 0.1 mgmL^{-1} aqueous solution of obtained CDs (Sample B).

Figure 15. CDs solution (0.1 mg mL^{-1}) of sample B (left) and water (right) when view under a 4-Watt, 254/365 nm UVGL-15 Compact UV lamp.

The Fluorescence (FL) Spectroscopy Results

The fluorescence analysis of CDs was also done using 0.1 mg mL^{-1} aqueous solution of the sample. It was observed that CDs exhibited an excitation dependent fluorescence. The CDs solution (0.1 mg mL^{-1}) from sample A was excited at different wavelengths from 320 nm – 380 nm (Fig. 16). The emission maximum was at 450 nm at an excitation wavelength of 360 nm. The emission at 360 nm appears to be highest, while emission at excitation 320 nm showed the lowest intensity. The FL result explains why aqueous solution of CDs shows a blue luminescence in the presence of a hand-held UV lamp.

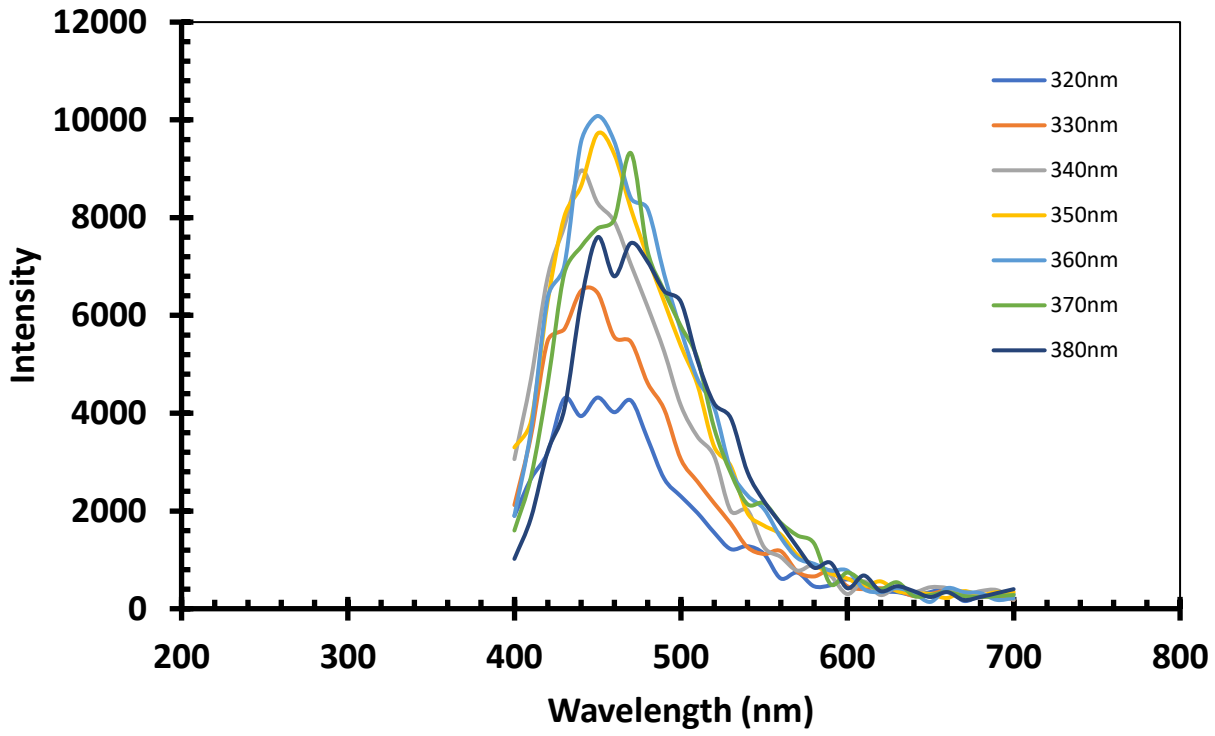

Figure 16. Fluorescence spectra of CDs (Sample A) at different excitation wavelength (320 nm – 380 nm).

The fluorescence analysis of CDs sample B was also investigated at wavelengths excitation of 320 nm – 380 nm (Fig. 17). For sample B, the maximum emission was also at 450 nm at an excitation wavelength of 360 nm. The emission at 360 nm appears to be highest, while emission at excitation 320 nm showed the lowest intensity. This result is very much similar to sample A CDs. The only noticeable difference is the intensity of the peaks. The emission maximum peak in sample B is higher than sample A.

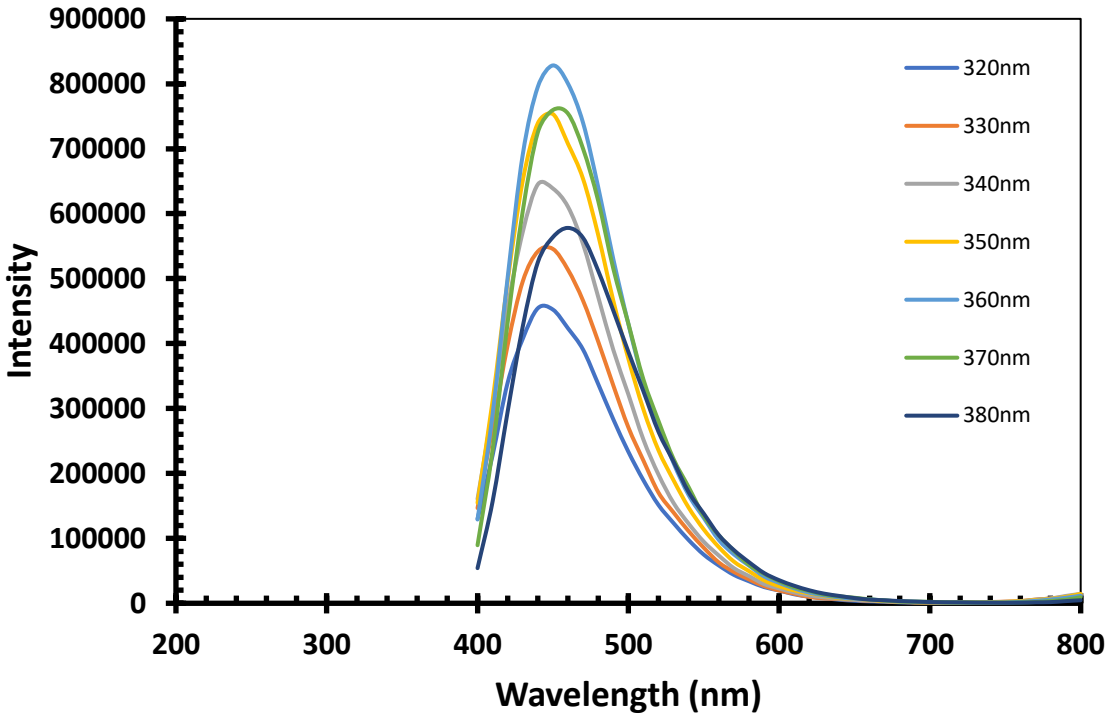

Figure 17. FL spectra of CDs (Sample B) at different excitation wavelength (320 nm – 380 nm).

The UV and FL results of the CDs samples showed that changing the ratio of the starting materials could have a slight impact on the optical properties of CDs – the intensity of the FL spectra are higher in sample B than in sample A as shown in Figure 16 and 15 respectively.

FTIR Results

The FTIR analysis was carried out for determination of the possible functional groups present. Few milligrams of the pure solid sample were taken for the analysis. As shown in Figure 18 below, the FTIR spectrum shows a very strong peak at 1693 cm^{-1} which reveals the presence of a carbonyl carbon (C=O). The presence of a C-H stretching is also confirmed with a peak at 2939 cm^{-1}. The broad absorption peak from 3000 – 3483 cm^{-1} indicates the presence of O-H/N-H functional group on the surface of the CDs. In the fingerprint region, the peak at 1404 cm^{-1} corresponds to O-H bending vibrations.

The very strong peak at 1693 cm^{-1} corresponds to the C=O stretch of carboxylic acid, which could be explained due to the high ratio of citric acid to ethylenediamine used in the synthesis of sample A.

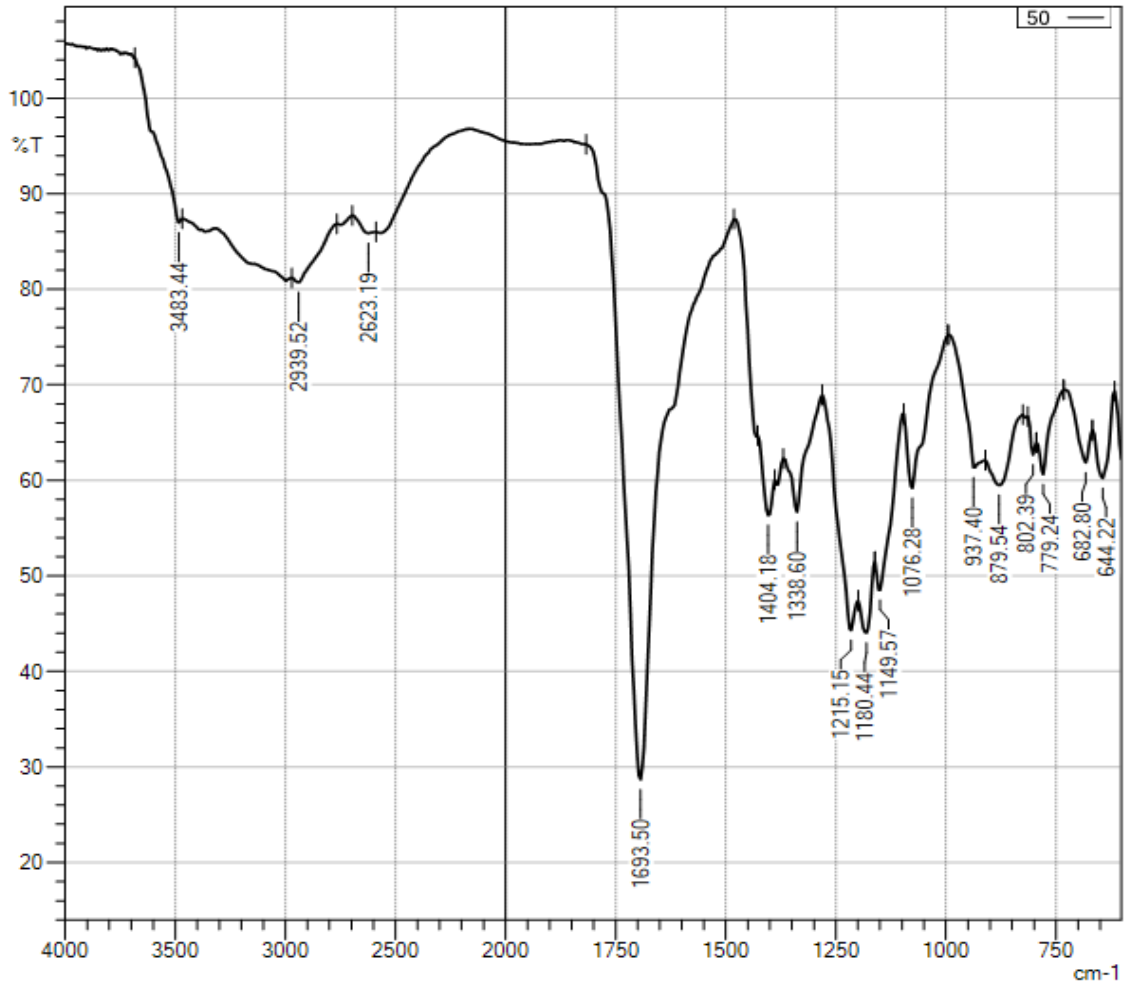

Figure 18. FTIR spectrum of CDs (Sample A).

On the other hand, the FTIR spectrum of CDs from sample B (Figure 19) shows the C=O absorption peak at 1651 cm^{-1}. Compared to sample A, the C=O stretch of sample B is less strong

or broad. The very strong peak at 1539 cm^{-1} represents N-H deformation and C-N stretching vibration of amide.[67] The spectra of sample B shows stronger and broad N-H stretching peak compared to sample A. This could be because the precursor was used in the same ratio of starting materials which allow for more primary amine or amide groups in sample B. The broad absorption peak at 3228 cm^{-1} represents N-H/O-H group in primary amine and carboxylic acid, while the peaks at 1435 cm^{-1} represent the C-H asymmetric stretch.

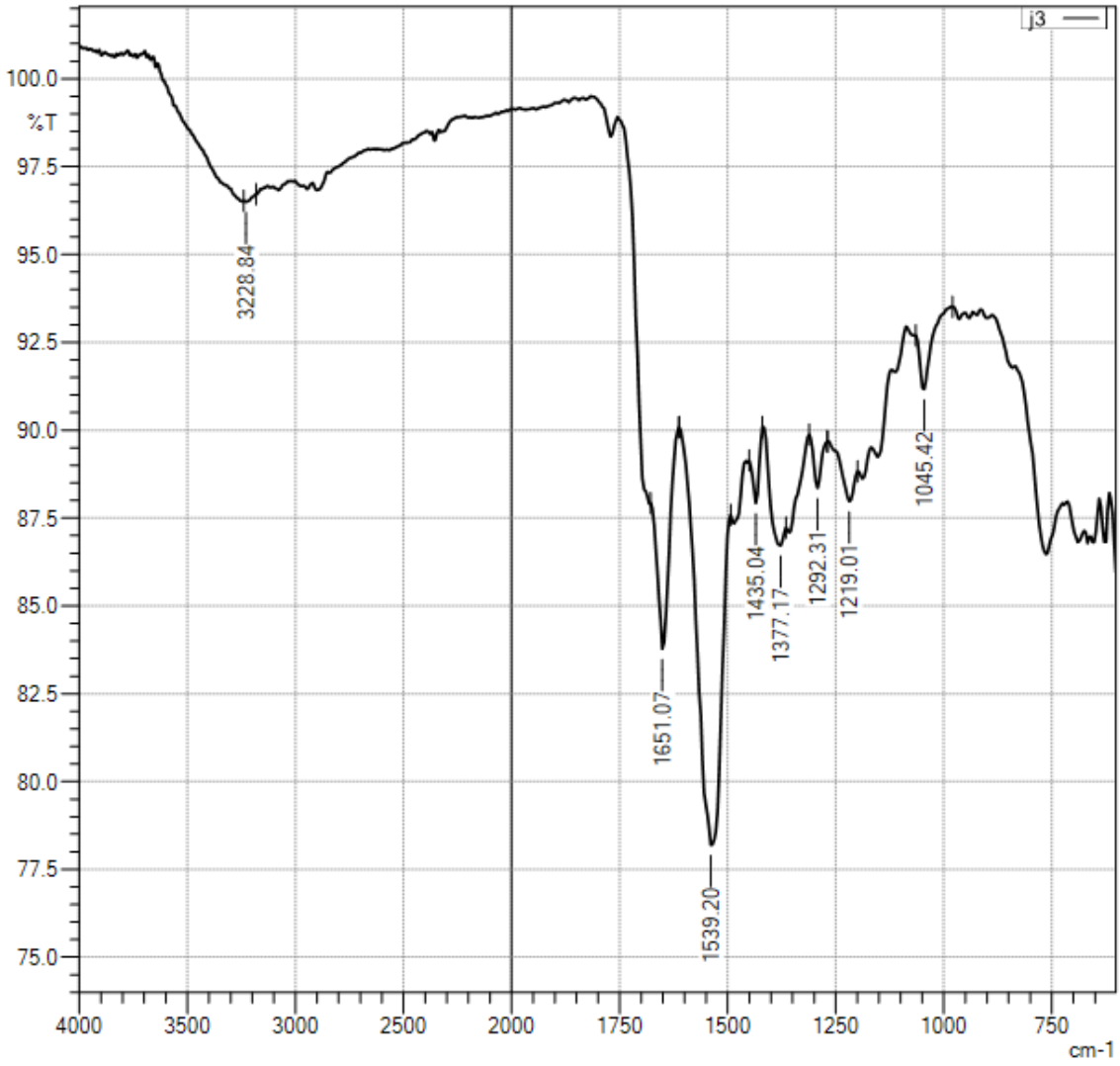

Figure 19. FTIR spectrum of CDs (Sample B).

The FTIR spectra obtained for CDs were compared to citric acid which was the dominant precursor in the starting material used. First, the absorption peak of C=O for citric acid is at 1743 and 1697 cm^{-1} while the C=O peak for sample A and B are at 1693 cm^{-1} and 1651 cm^{-1} respectively. Additionally, the O-H functional group of citric acid as shown in Figure 20 is sharp and medium with an absorption peak at 3286 and 3495 cm^{-1}.The peaks are comparably broad and medium for –OH group in the CDs samples. Even though both CDs samples showed the presence of N-H/O-H bonds, the peak intensity and shape are different compared to citric acid. Nonetheless, the C-O absorption peaks in the fingerprint region at 1215 cm^{-1} are similar in all three spectra. Shoujun Zhu and his group showed similar IR spectra for CDs prepared using the hydrothermal treatment from citric acid and ethylenediamine.[63] The IR spectra show that sample A is more similar to citric acid particularly at the C=O absorption band, this may be because it has it has excess of citric acid compared to ethylenediamine.

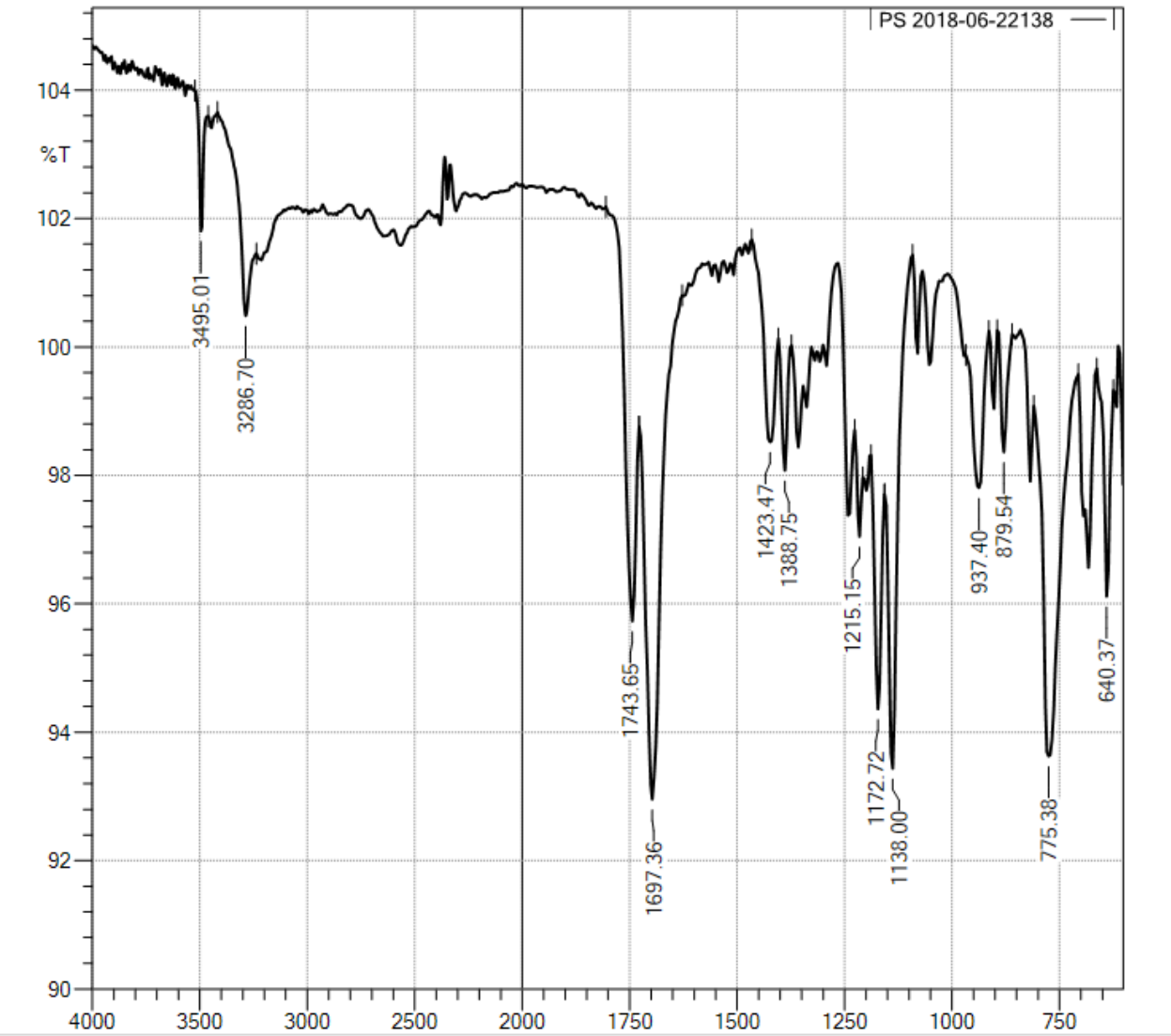

Figure 20. FTIR spectra of citric acid

Synthesis of FA-CDs

Synthesis of the FA-CDs complex was completed using EDC/NHS coupling reaction (carbodiimide crosslinker). The amine group on the surface of the CDs was conjugated with the carboxylic acid group in folic acid.[67] This method allows for the creation of a non-cleaveable covalent bond between CDs and FA. The reaction was carried in two steps as shown in Scheme 2 and 3 below.[91]

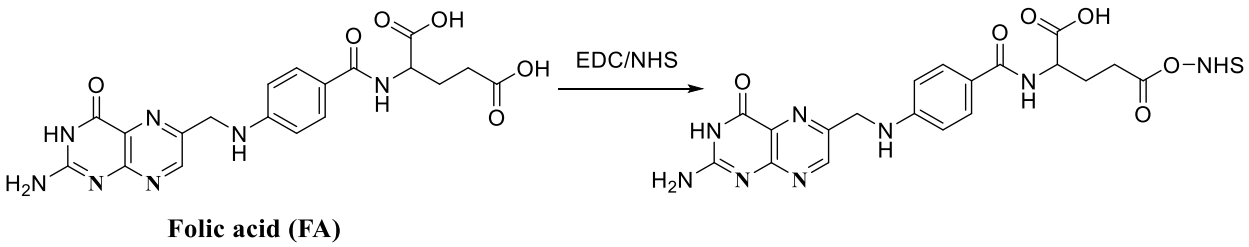

Scheme 2. Activation of the carboxylic acid functional group using EDC and NHS.[91]

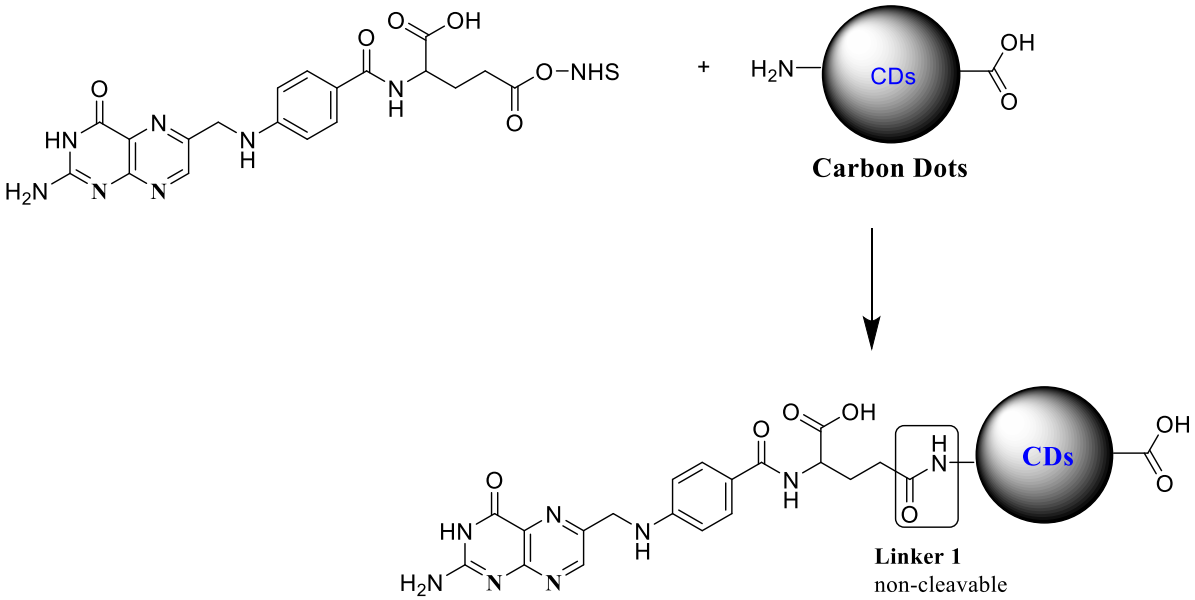

Scheme 3. Formation of a non-cleavable linker between CDs and FA. (The drawings in the scheme are not according to the actual scale and ratio. For clarification, only one carboxylic acid and one amine group are shown for CDs; only one FA is shown to react with CDs, and only a few of Dox attach to FA-CDs).[91]

The first step of the reaction typically involves activation of the acid functional group of folic acid using EDC and NHS. This allows for the easy conjugation of the amine functional group of CDs. The reaction was carried out in a PBS buffer solution the whole time to ensure that the reactants remain stable . The resulting solution from the experiment was subjected to dialysis to remove unreacted reagents and for purification of the sample. The desired solid

products FA-CDs were obtained after purification using dialysis and lyophilization. The drying process of FA-CDs of both samples took relatively the same time around 48 hours. And powder yellow solid products were obtained with decent yields approximately 40% wt. The desired product were stored for further characterization.

UV-vis and FL spectroscopy result of FA-CDs (from CDs Sample A and B)

UV-vis Analysis of FA-CDs (from CDs sample A)

The FA-CDs complex showed three characteristics absorption at 201 nm, 279 nm, and 342 nm. The absorption peak at 201 nm and 342 nm are evidence of the presence of CDs, while the peak at 279 nm is characteristic of FA as reported by existing literature.[67,69] This results represents the likely conjugation of CDs to FA. The UV-vis absorption spectrum was compared to spectrum of pure FA solution, using the same concentration (0.1 mg mL^{-1}) as shown in Figure 21. The FA-CDs from CDs sample A have characteristic absorption peaks of FA at 290 and 342 nm. and the characteristic absorption peak of CDs sample A at 344 nm. Those data indicate the successful functionalization of FA onto CDs surface. The absorption peaks of FA-CDs at 342 nm are enhanced since both free FA and CDs have characteristic absorption peak in this region. Also, it was noted that the absorbance readings at the higher end of the spectrum from 300 nm – 790 nm are quenched in FA-CDs.

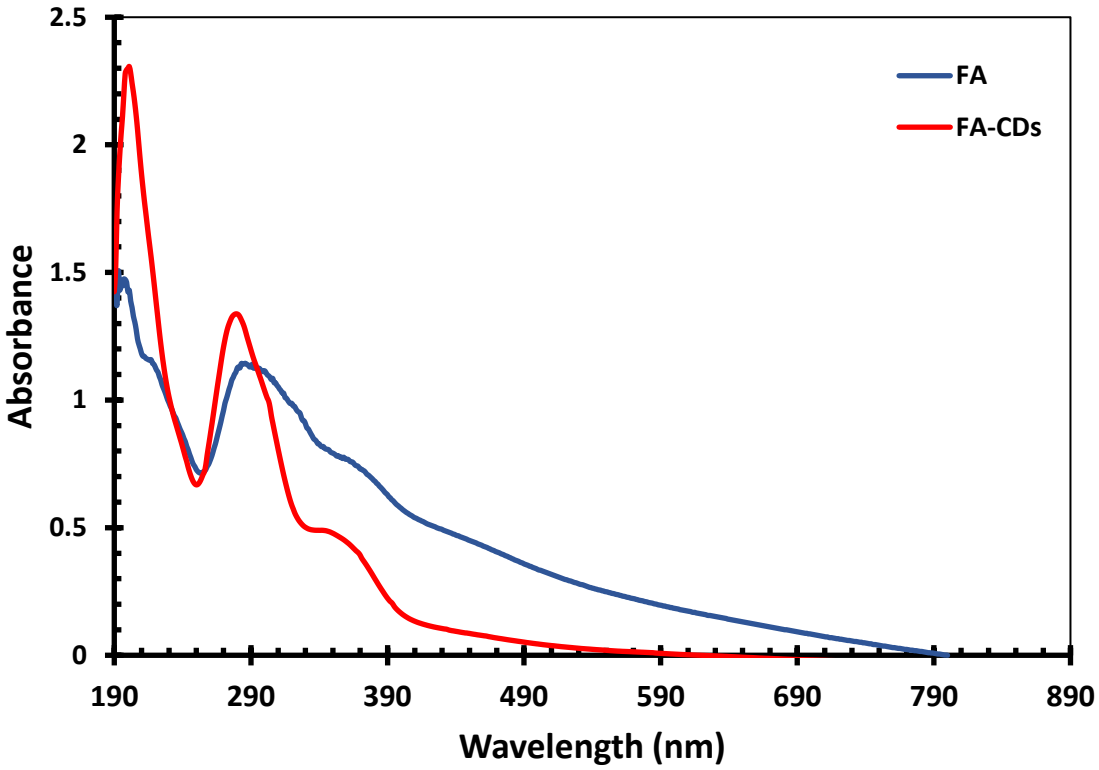

Figure 21. UV-vis of obtained FA and FA-CDs (from CDs Sample A).

UV-vis Analysis of FA-CDs (from CDs Sample B)

The absorbance results elucidated that the product FA-CDs contains both CDs and FA. Detailed analysis of the absorbance spectra (Figure 22) showed that the spectra of pure FA, pure CDs from sample B, and FA-CDs are comparable. In addition to the unique absorbance of FA at 283 nm,[67] the FA-CDs showed the absorbance peaks at 201 nm and 340 nm corresponding to CDs. The UV-vis spectra data for both FA-CDs are similar, but the intensities are different. The FA-CDs from sample A showed characteristic absorbance spectra at 201 nm, 282 nm and 342 nm, while the FA-CDs from sample B showed absorbance peak at 201 nm, 283 nm and 340 nm.

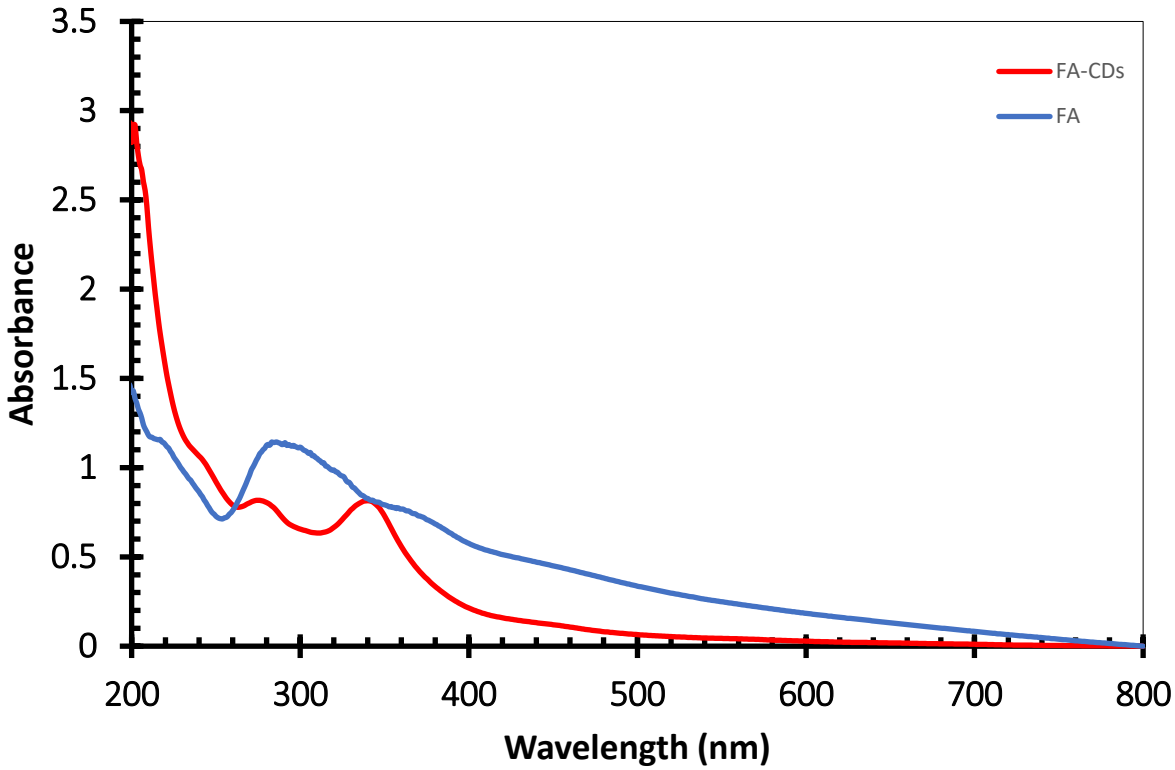

Figure 22. UV-vis spectra of obtained FA & FA-CDs (from CDs Sample B).

FL Spectroscopy of FA-CDs (from CDs Sample A)

The FL spectra of FA and FA-CDs were done as shown in Figures 23 and 24 to obtain the emission wavelength of the two samples. The maximum emission was at the excitation wavelength of 360 nm and the maximum emission peaks are at 440 nm and 450 nm for FA and FA-CDs respectively. Additionally, it was noted that the emission intensity of FA-CDs is enhanced compared to pure FA or CDs sample A.

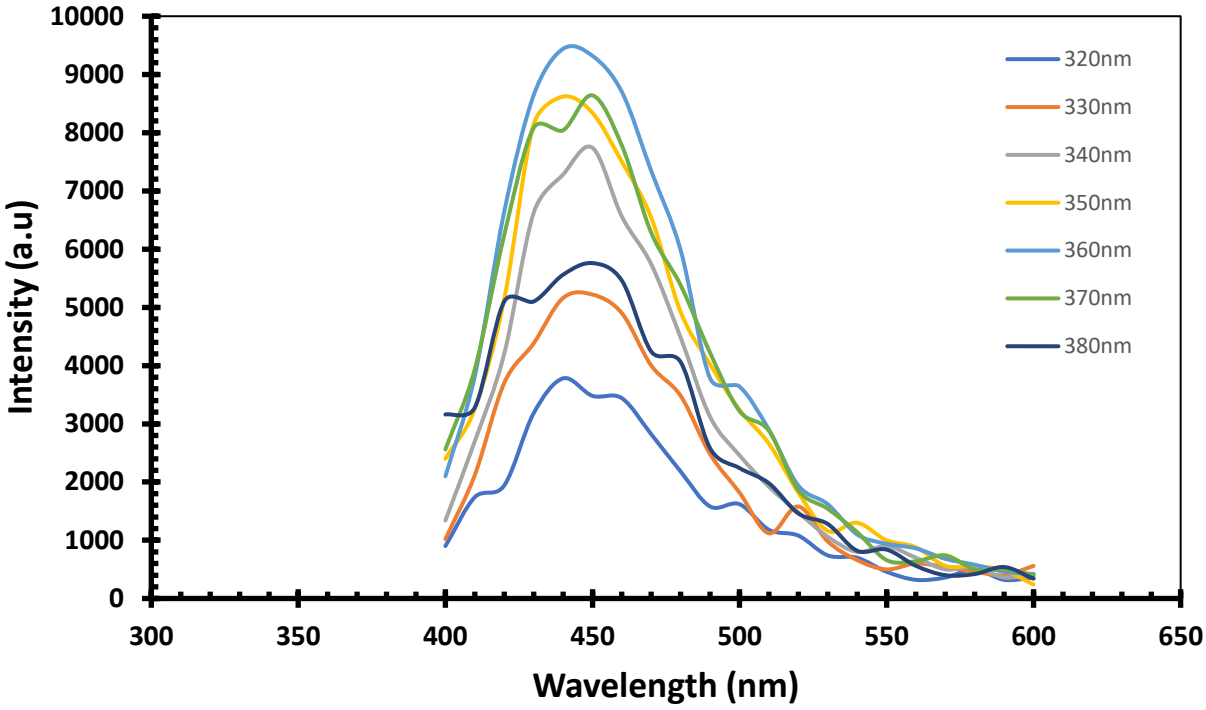

Figure 23. FL spectra of pure FA (0.1 mg mL^{-1}) at different excitation wavelength (320 nm – 380 nm).

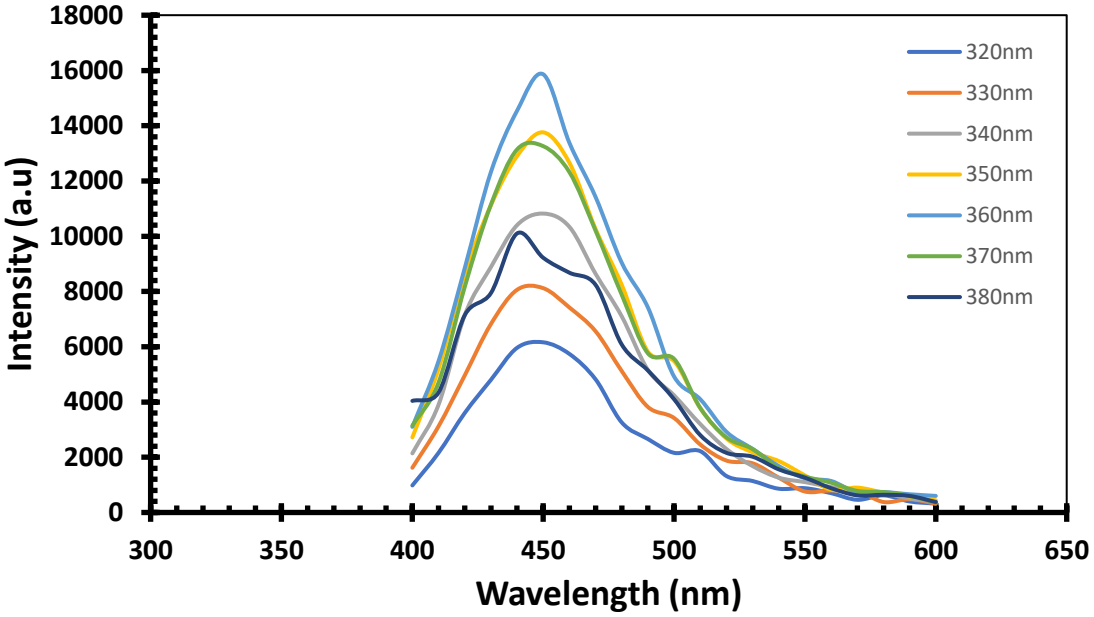

Figure 24. FL spectra of FA-CDs 0.1 mg mL^{-1} (from CDs Sample A) at different excitation wavelength (320 nm – 380 nm).

FL Spectroscopy of FA-CDs (from CDs Sample B)

The FL intensity of FA-CDs (prepared from CDs sample B) is somewhat similar to the FA-CDs prepared from sample A. Both FA-CDs samples exhibited an excitation-dependent wavelength property by having the maximum emission peak at 450 nm at an excitation wavelength of 340 and 360 nm respectively as shown in Figure 24 and 25, the λ_{max} here appears to shift at different excitation. The major difference is the emission peak intensity of the FA-CDs from sample B which is much higher than FA-CDs from sample A at all excitation wavelengths.

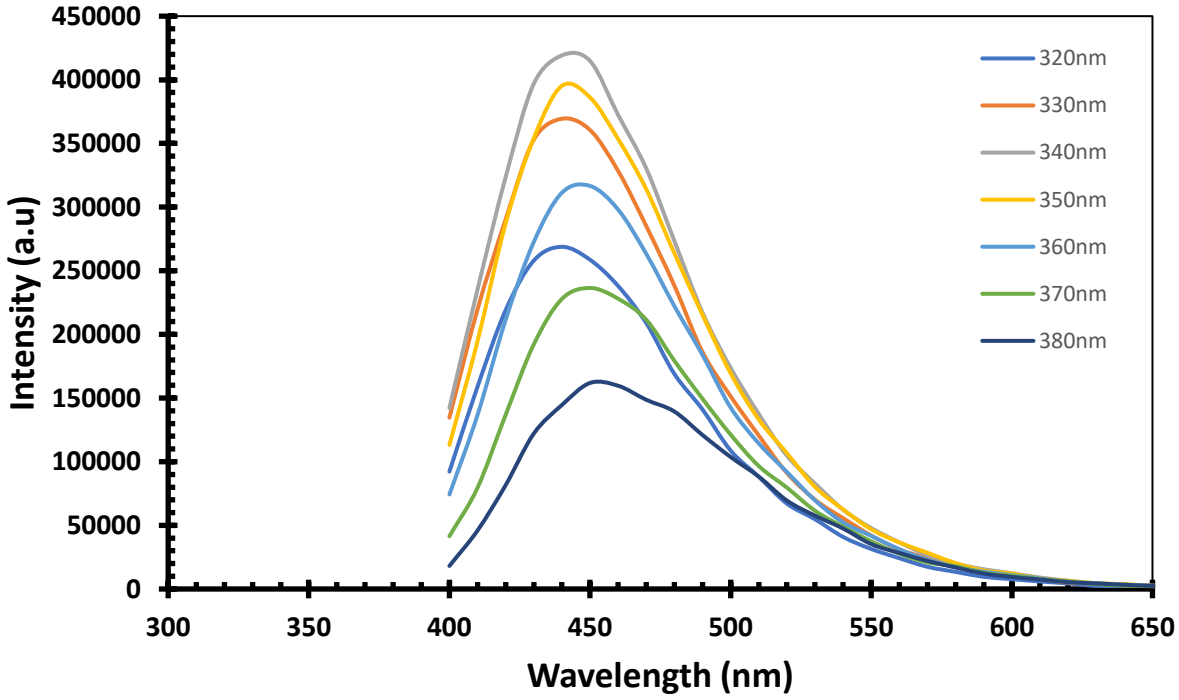

Figure 25. FL spectra of FA-CDs 0.1 mg mL^{-1} (from CDs Sample B) at different excitation wavelength (320 nm – 380 nm).

FTIR Results of FA

Figure 26 below shows FTIR spectroscopy of pure FA. The spectrum has the characteristics absorption peaks at 1639 cm^{-1} corresponding to C=O of amide ($-CONH_2$), and at 1693 cm^{-1} corresponding to C=O of carboxylic acid (-COOH). The peaks at 1604, 1485, 1519 cm^{-1} correspond to phenyl and pterin rings.[67] The peak at 2927 cm^{-1} corresponds to C-H stretching, and the peaks at 3097, 3545 cm^{-1} matches that of O-H of carboxylic acid and N-H stretching of primary amine.

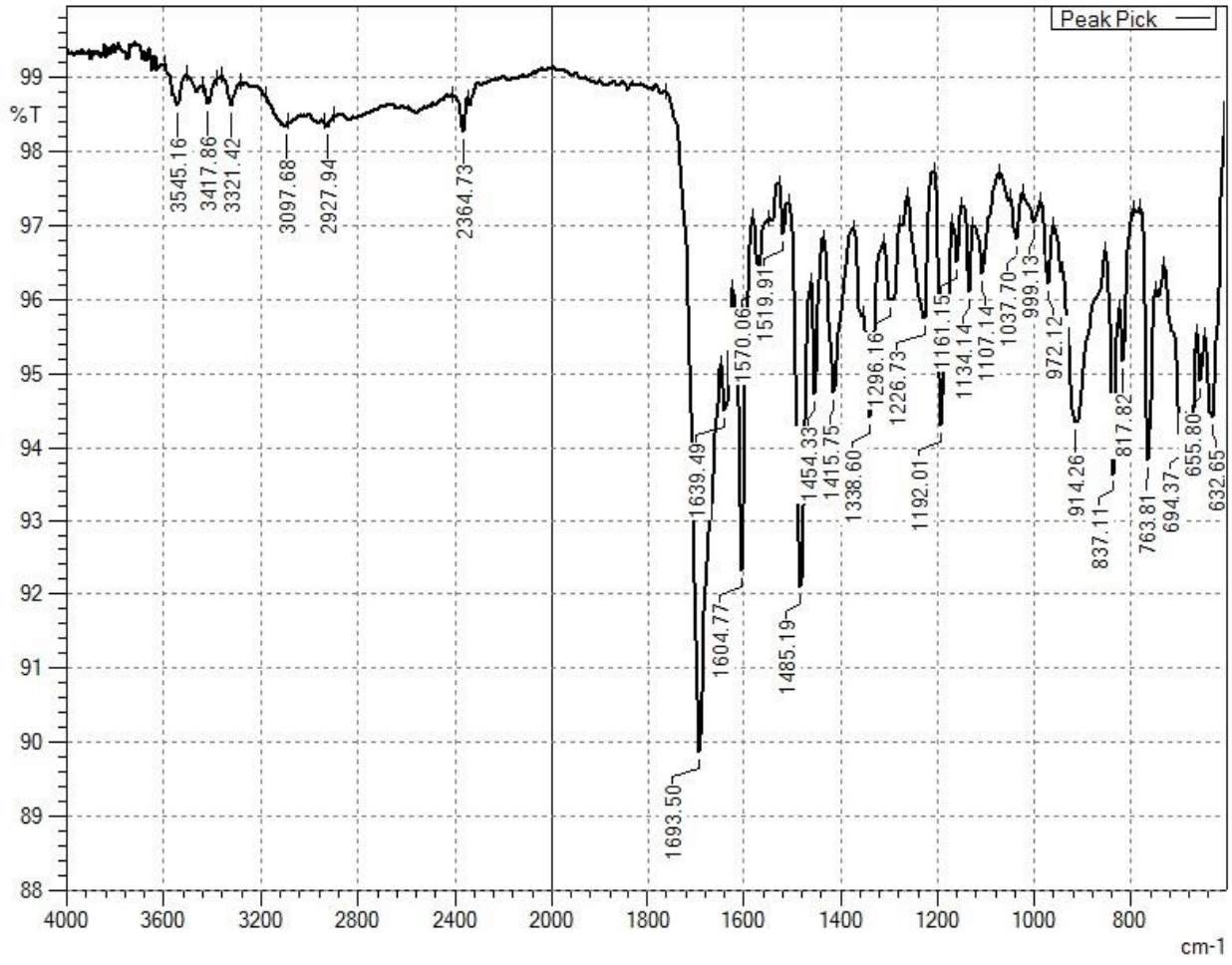

Figure 26. FTIR spectra of pure FA.

FTIR Results of FA-CDs (from CDs sample A)

Both FA-CDs samples show the characteristic peaks present in its precursor – CDs and FA. In the FA-CDs (from sample A CDs) IR spectrum, there are noticeably peaks at two different amides absorption band (I and II) at 1689 cm^{-1} (C=O) and 1639 cm^{-1} (N-H bending) The peaks at 1604, 1481, 1516 cm^{-1} corresponds to phenyl and pterin rings. The presence of C-H stretching frequency at 2839 and 2927 cm^{-1} was also observed, the band observed at 1180 cm^{-1} which is absent in the spectra of pure FA, corresponds to C-O-C stretching.[67] The peaks from 2839 – 3541 cm^{-1} appears more broad in the spectra of FA-CDs compared to pure FA.

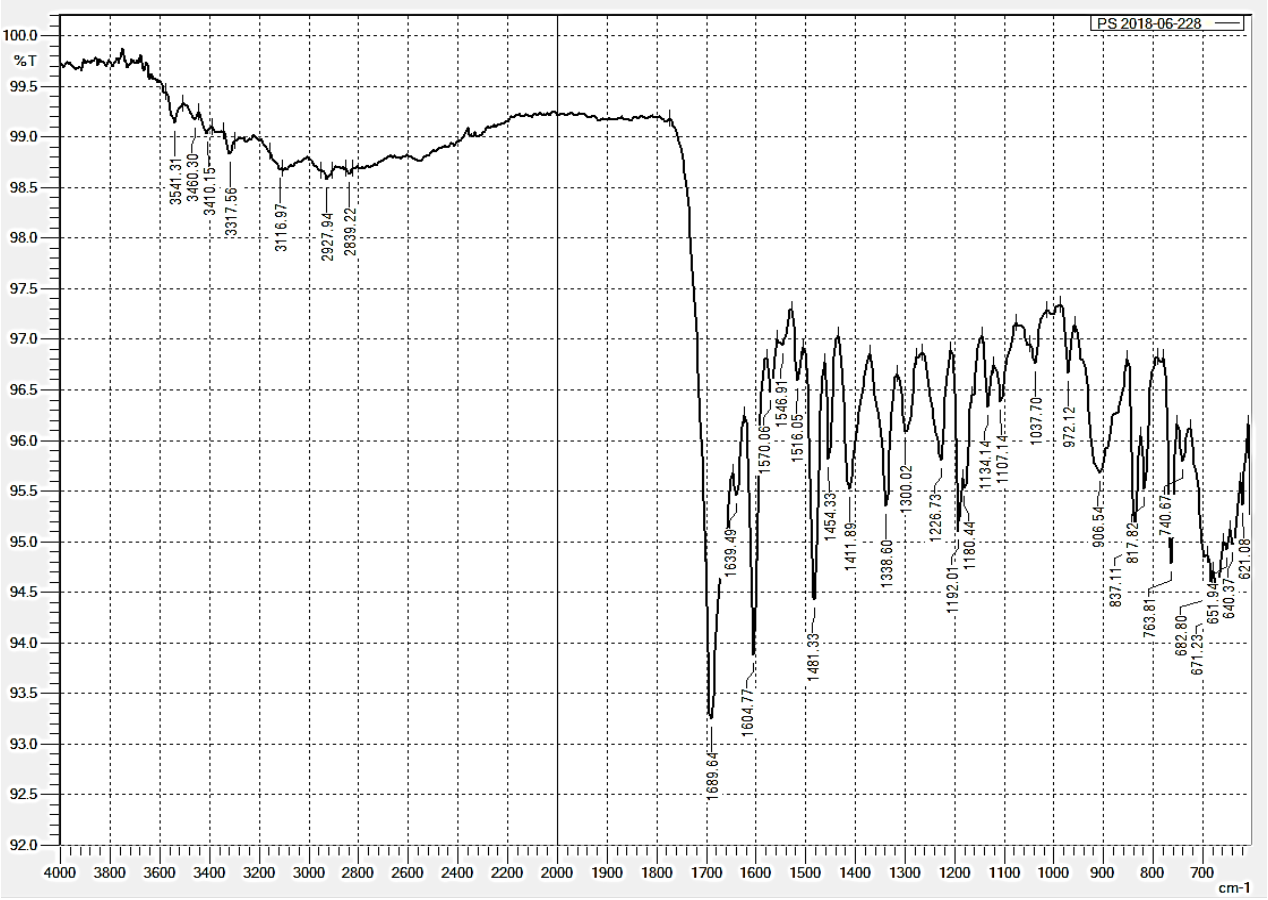

Figure 27. FTIR spectra of FA-CDs (from CDs sample A).

FTIR Results of FA-CDs (from CDs sample B)

For the FTIR spectrum of FA-CDs (prepared from CDs sample B), the absorption peaks at 1604 cm^{-1}, and 1485 cm^{-1} representing the presence of C=C can be seen in the FA spectrum. The C=O band and the N-H bending peak appear at 1685 cm^{-1}, 1639 cm^{-1} respectively, which are similar to the FA-CDs from sample A. From the comparison data of FA and FA-CDs, it confirms that the attempt to conjugate CDs to FA was successful.[92,93]

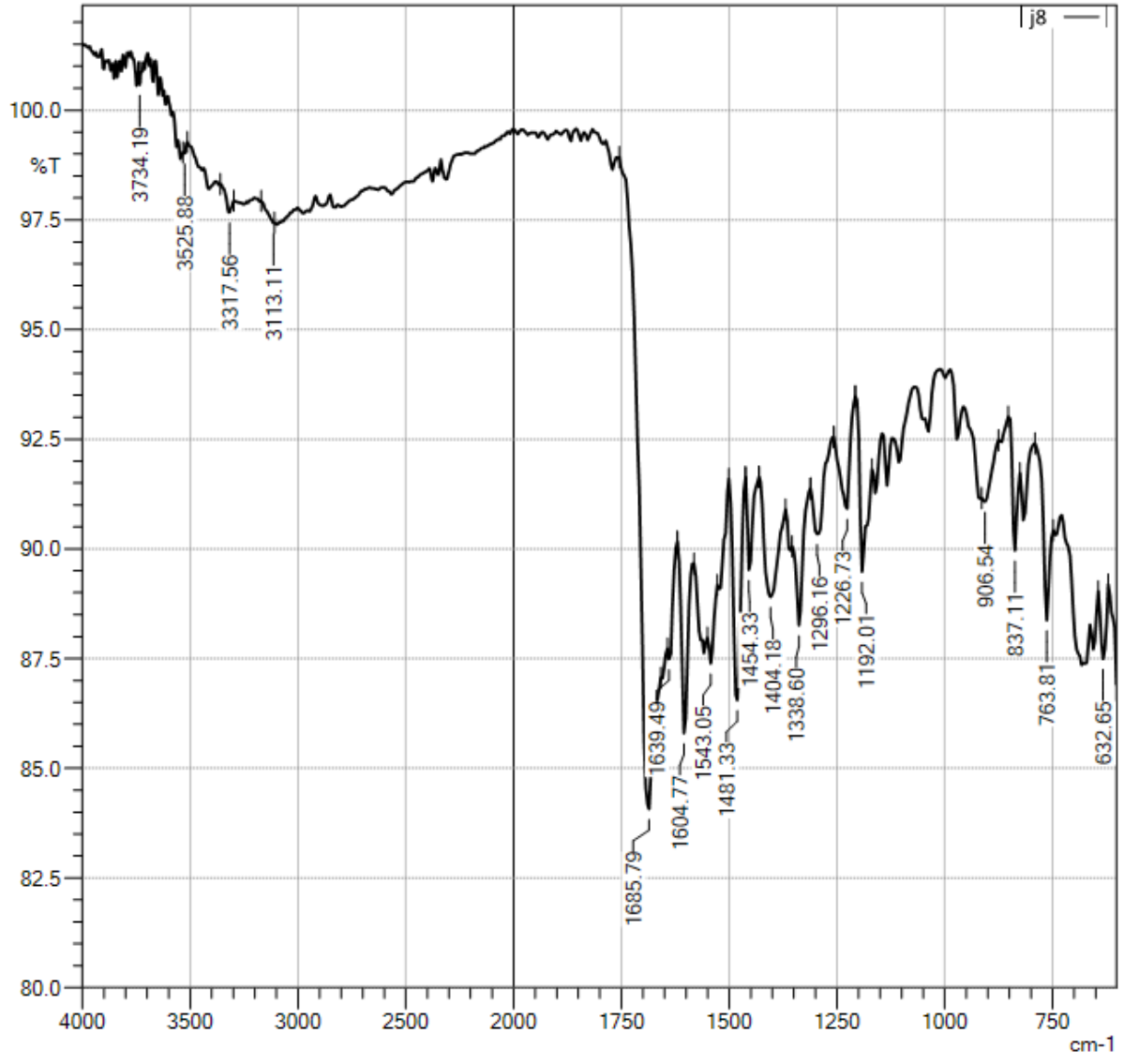

Figure 28. FTIR spectra of FA-CDs (from CDs sample B).

Synthesis of FA-CDs-Dox

The synthesis of the FA-CDs-Dox NPs was achieved due to Dox ability to exist as a cation in aqueous solution of pH 7.4, at which the amino group is protonated.[80] Thus, Dox can be potentially loaded on the negatively charged NPs via electrostatic interaction and π-π stacking.[14,30,81] Scheme 4 below shows the reaction scheme between FA-CDs and Dox. Since Dox has a unique UV-vis absorbance peak, it is possible to confirm the successful formation of the FA-CDs-Dox complex using spectroscopic techniques.

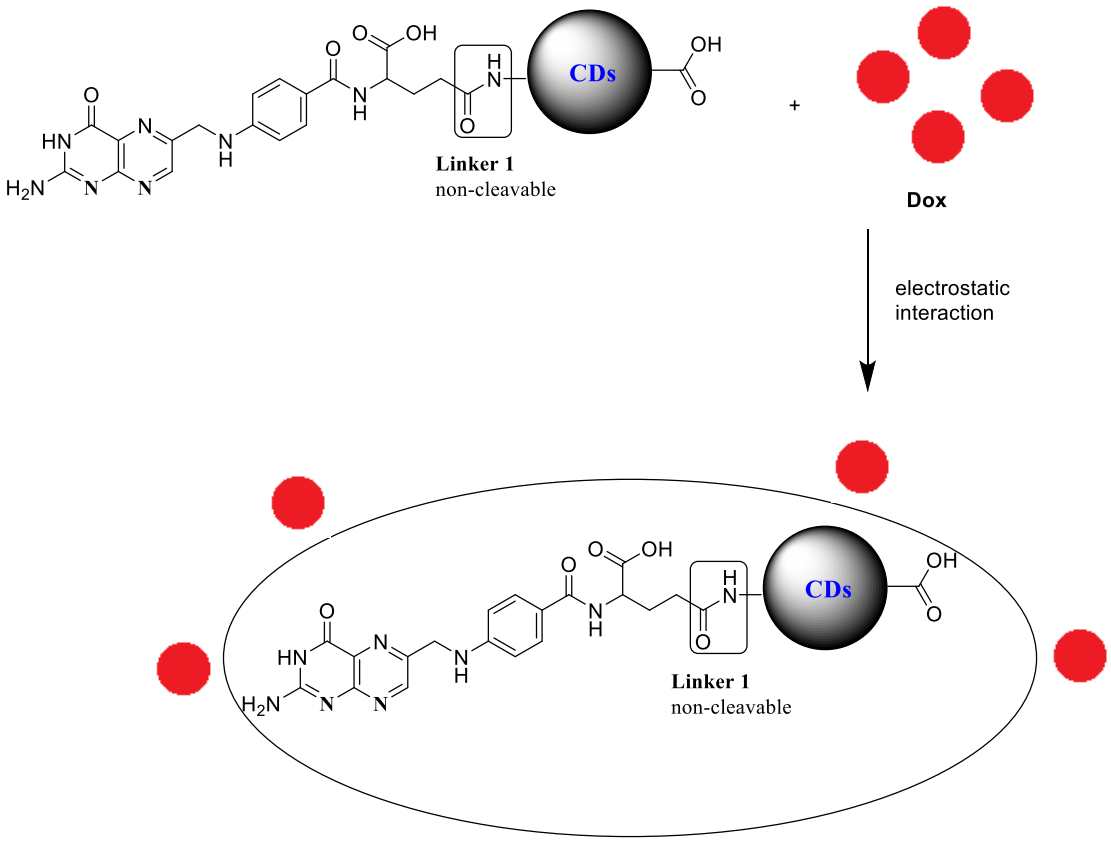

Scheme 4. Electrostatic interaction of FA-CDs and Dox. The drawings in the scheme are not according to the actual scale and ratio. For clarification, only one carboxylic acid and one amine

group are shown for CDs; only one FA is shown to react with CDs, and only a few of Dox attach to FA-CDs.[91]

UV-vis Analysis Result of FA-CDs-Dox (prepared from CDs Sample A)

Dox has a unique absorbance peak at 480 – 485 nm,[11,88,94] the similar peak at 480 nm is quenched in our prepared FA-CDs-Dox. The solution of FA-CDs-Dox (prepared from CDs sample A) also has the absorbance peaks characteristic of FA-CDs, at 281 nm and 344 nm.

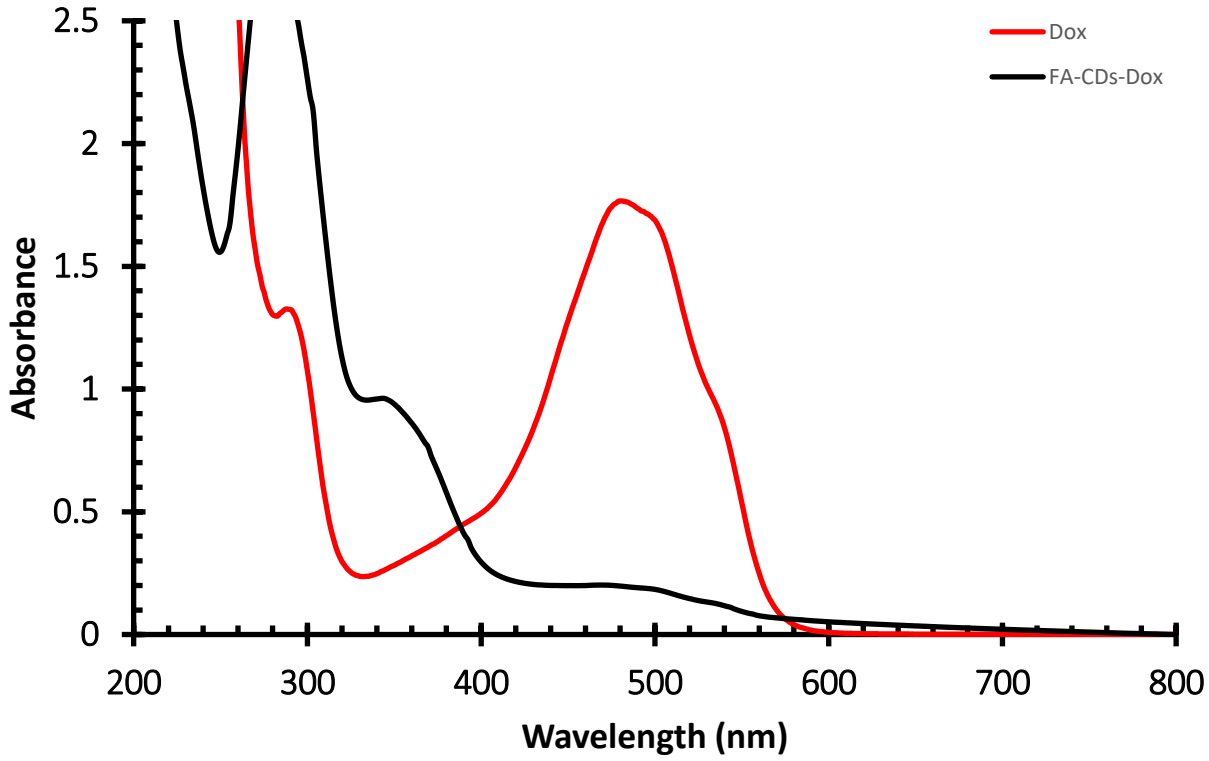

Figure 29. UV-vis spectra of 0.1 mgmL^{-1} of pure Dox and FA-CDs-Dox (from sample A).

UV-vis Analysis Result of FA-CDs-Dox (from CDs Sample B)

Similar results were observed in FA-CDs-Dox from sample B with slightly differences. There is an absorbance peak at 480 nm in FA-CDs-Dox characteristic of Dox. It is noticeable that the absorbance at this wavelength is quenched in FA-CDs-Dox compared to Dox for both FA-CDs-Dox samples. The solution of FA-CDs-Dox also shows the characteristic absorbance peaks of FA-CDs, at 290 nm and 340 nm, but with lower intensity compared to the other series.

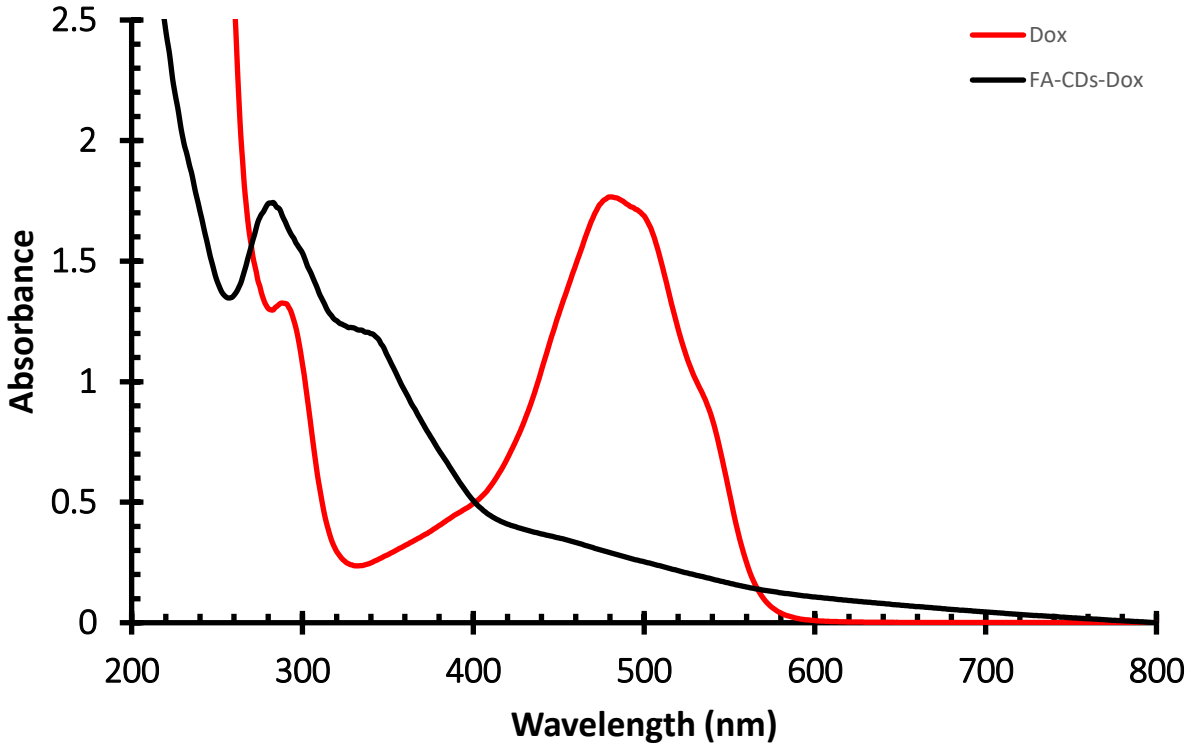

Figure 30. UV-vis spectra of pure Dox and FA-CDs-Dox (from sample B).

FL Spectroscopy of FA-CDs-Dox

It was observed that the maximum emission of FA-CDs-Dox (from CDs sample A) was at 440 nm at an excitation 360 nm, while the excitation at 320 nm has the lowest emission

intensity. The maximum emission of FA-CDs-Dox (from CDs sample B) was at 440 nm at an excitation of 340 nm. It was noticed that once the maximum emission is reached at an excitation of 340 nm, the emission intensity decreases for every 10 nm increase in the excitation wavelength.

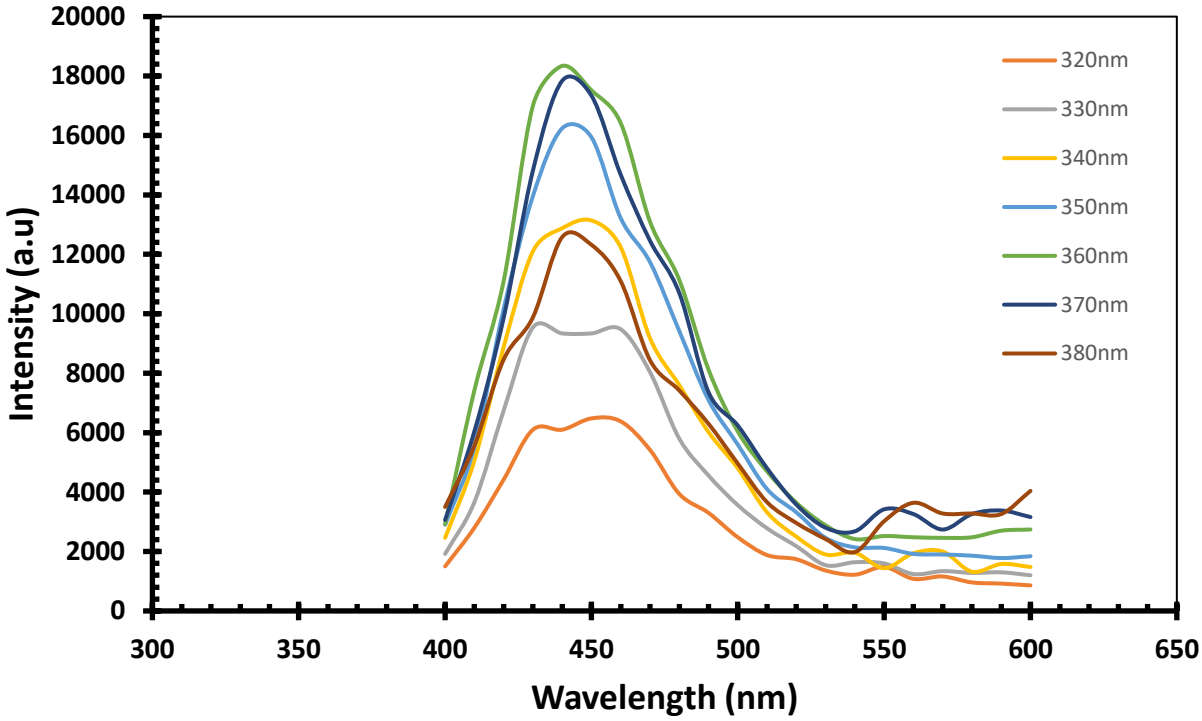

Figure 31. FL spectra of FA-CDs-Dox 0.1 mg mL^{-1} (from CDs sample A) at different excitation wavelength (320 nm – 380 nm).

Both FA-CDs-Dox exhibits an emission λ_{max} at 440 nm at excitation wavelength of 340 and 360 nm respectively. However, the emission intensity is obviously higher for FA-CDs-Dox (from CDs sample B) than for FA-CDs-Dox (from CDs sample A). Figures 31 and 32 shows the FL spectra of FA-CDs-Dox (from CDs samples A & B) respectively.

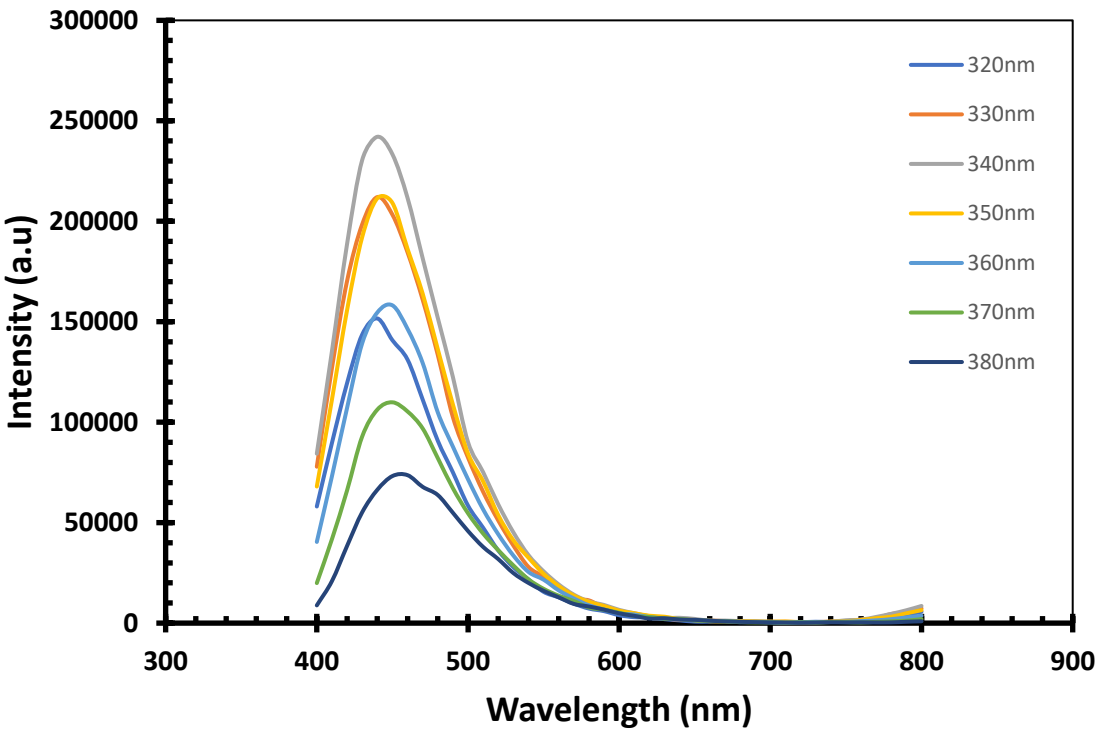

Figure 32. FL spectra of FA-CDs-Dox 0.1 mg mL^{-1} (from CDs sample B) at different excitation wavelength (320 nm – 380 nm).

FTIR Results of FA-CDs-Dox (from CDs sample A)

As shown in figure 31 below, the FTIR spectrum of pure Dox shows characteristic absorption peak at 1728 cm^{-1} corresponding to C=O stretching vibrations. The peaks at 1234, 1616, 2897, 3317, 3522 cm^{-1} match C-O stretching, C=C stretching, C-H stretching, N-H stretching, and O-H stretching molecular vibrations respectively. For the new prepared FA-CDs-Dox from sample A (Figure 34), there are the absorption bands at 3105 - 3564 cm^{-1} corresponded to O-H and N-H stretching vibrations; the typical absorption band of C=O stretching vibrations can be observed around 1604 – 1685 cm^{-1}; the peak at 1296 cm^{-1} is characteristic of C-N stretching vibrations; and bands appearing at 1176 cm^{-1} can be assigned to C-O-C in stretching mode.

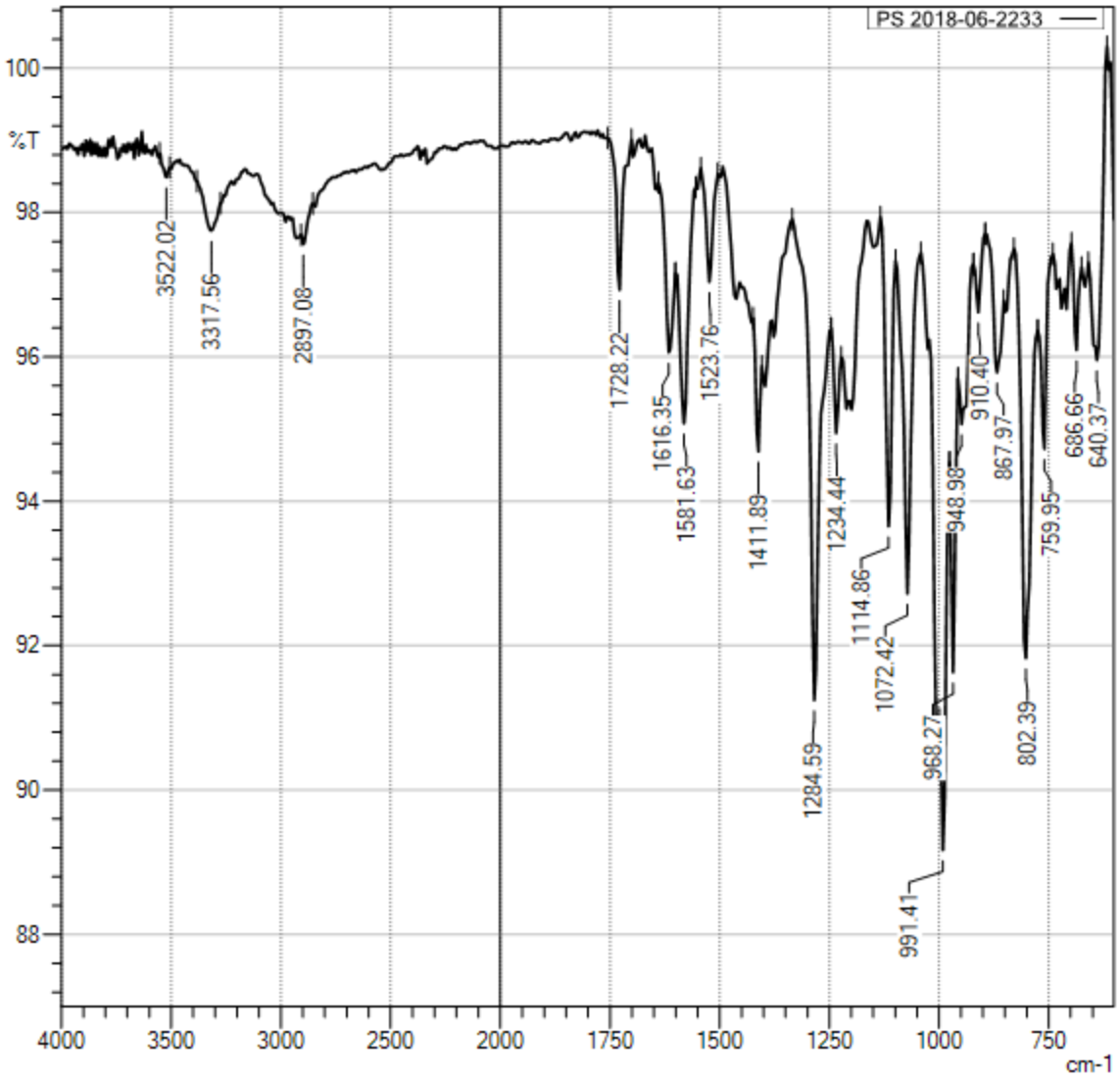

Figure 33. FTIR spectrum of pure Dox

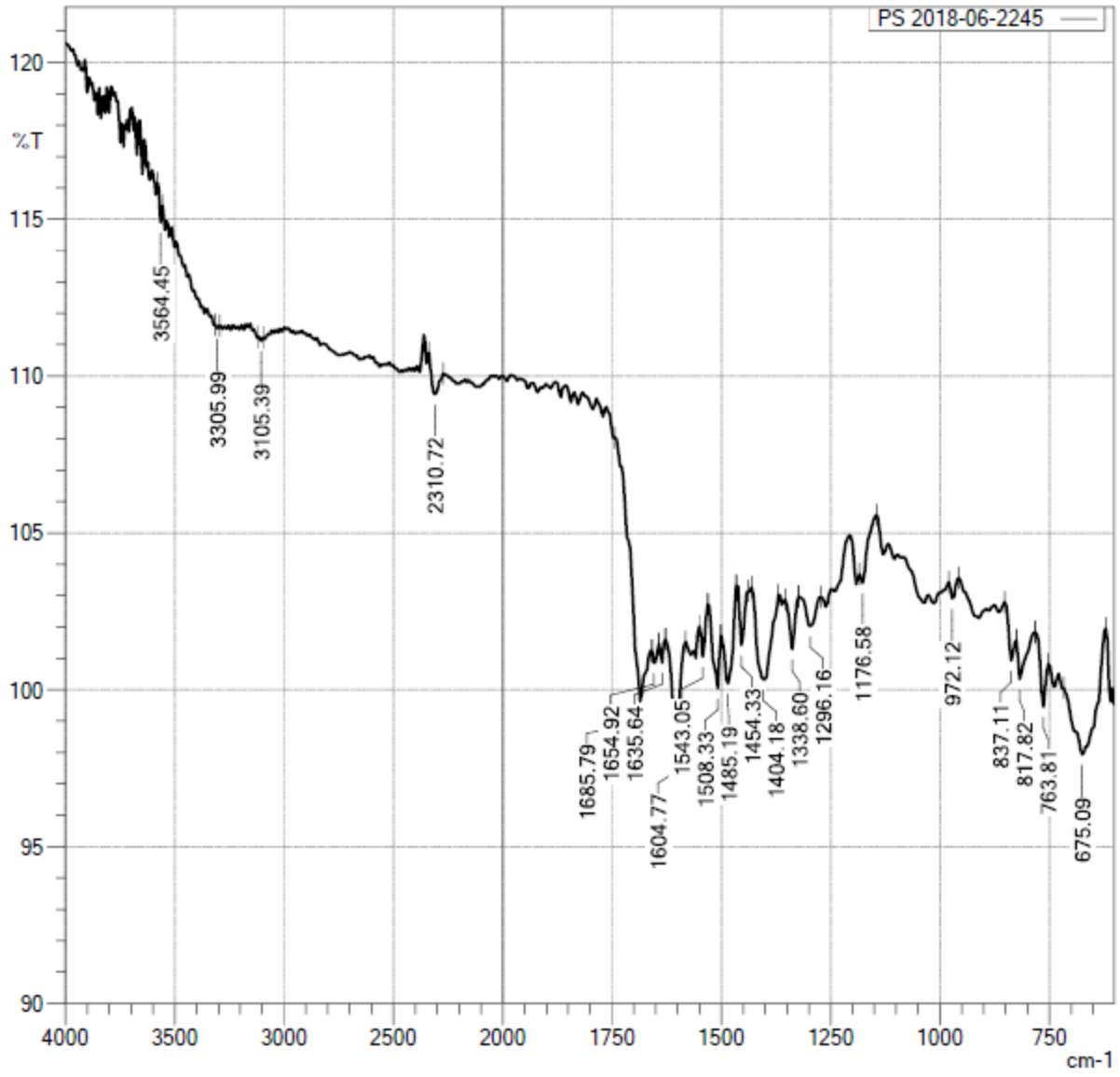

Figure 34. FTIR spectra of FA-CDs-Dox (from CDs sample A)

FTIR Results of FA-CDs-Dox (from CDs sample B)

The IR spectrum below (Figure 35) shows absorption peaks that indicates the evidence of conjugation of FA-CDs and Dox via electrostatic interaction. The broad peak at 3093 – 3321 cm^{-1} reveals the presence of O-H stretching vibration, and absorption peak at 2978 cm^{-1} represents the presence of C-H stretching vibrations. The peaks at 1689 cm^{-1} and 1651 cm^{-1}

corresponds to C=O and N-H of amide, while absorption peaks at 1539 cm^{-1} and 1134 cm^{-1} corresponds to N-H bending and C-O stretching molecular bonds respectively. Both samples showed absorption band at 3564 – 3093 cm^{-1} the amide peak band at 1689 – 1685 cm^{-1} for C=O and 1651 – 1654 cm^{-1} for N-H, peak at 1604 cm^{-1} and 1400 cm^{-1} appeared in both samples corresponding to C=C.

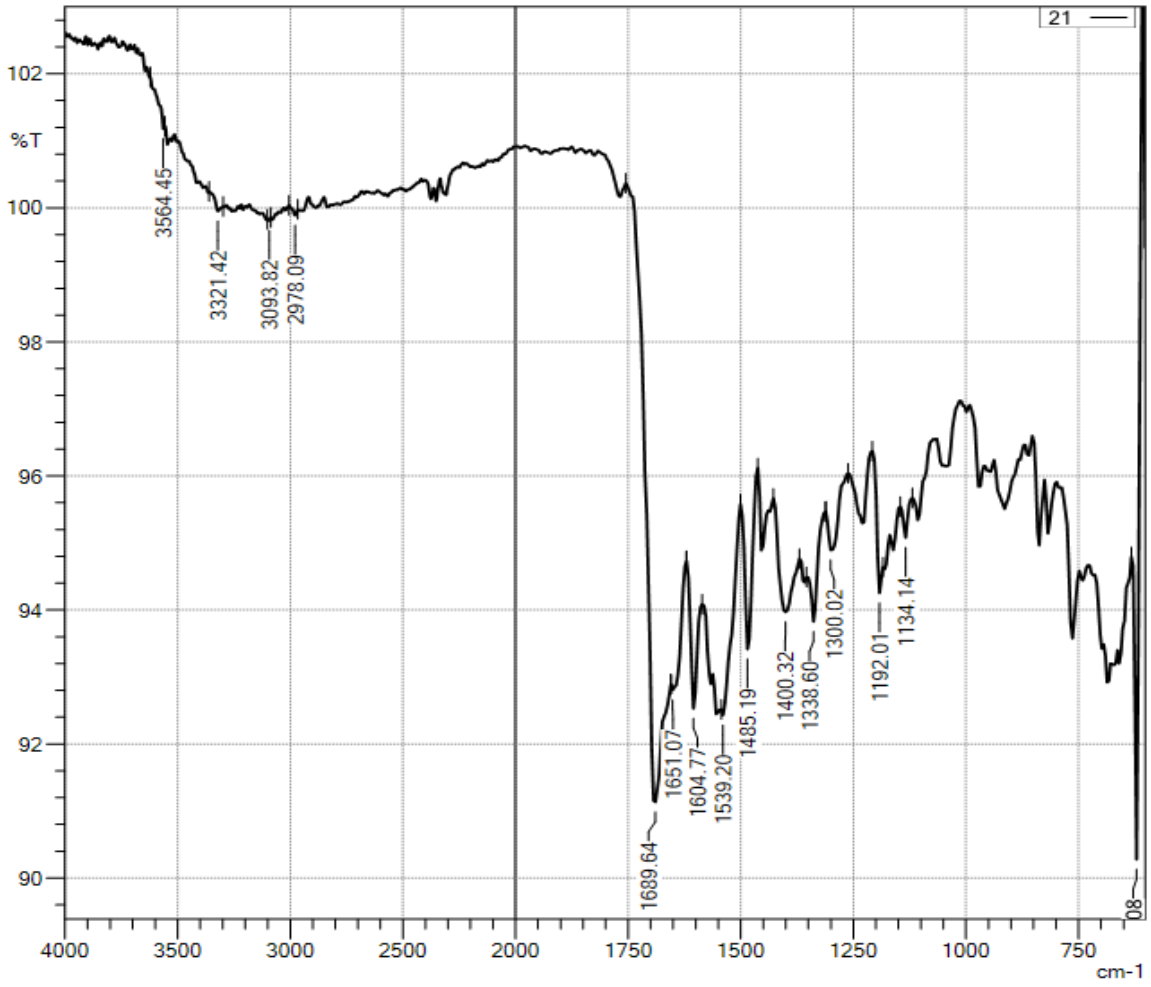

Figure 35. FTIR spectra of FA-CDs-Dox (from CDs sample B).

Determination of Concentration

The concentration of each component present in FA-CDs-Dox was determined using standard calibration curve. Standard solutions of different concentrations were prepared for FA-CDs and FA-CDs-Dox from FA and Dox. The UV absorbance values for each of the concentration was recorded at specific signature wavelength peculiar to each nanoparticle. After which, a calibration curve was set and the unknown concentration of each component of the final mixture of FA-CDs-Dox was determined using the known values of the absorbance and concentration of the standards.

Calibration Curve

Different concentration of Dox was prepared 0.075 mg mL^{-1}, 0.050 mg mL^{-1}, 0.025 mg mL^{-1}, 0.010 mg mL^{-1}, 0.005 mg mL^{-1}, 0.0010 mg mL^{-1}, and blank as shown in Table 3. The absorbance of the samples at 485 nm were taken and a standard calibration curve as shown in Figure 36 below was obtained.

Table 3. Different concentration of Dox and Absorbance Measured

Concentration (mg mL^{-1})	**Absorbance**
0.075	1.592
0.050	1.074
0.025	0.51
0.010	0.141
0.05	0.053
0.01	0.002
Blank	0.000

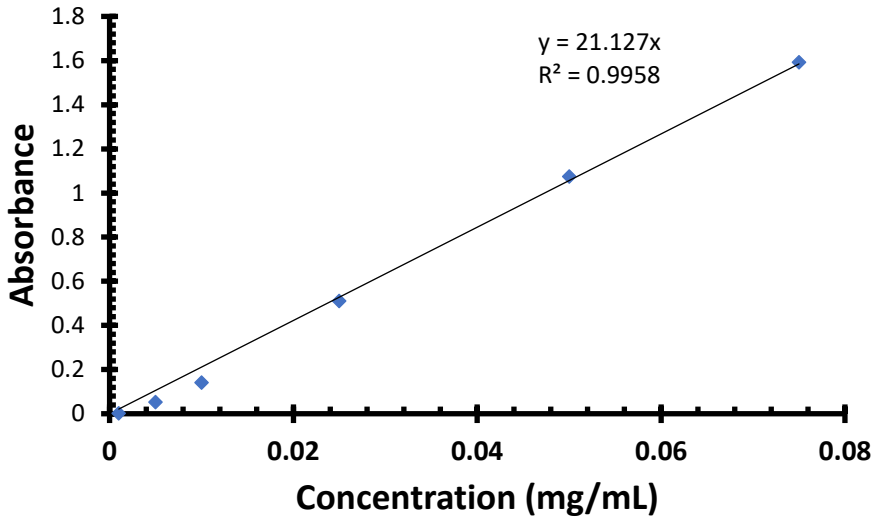

Figure 36. Calibration curve of Dox showing concentration (in mg/mL) against absorbance.

Calculation of Concentration of FA in FA-CDs (from CDs sample B)

The concentration of FA in FA-CDs was determined by using similar method described above, this involves measurement of absorbance of different known concentration of FA at the absorbance of 280 nm as shown in Table 4.

Table 4. Absorbance of Various Concentration of FA at 280 nm

Weight of FA used (mg)	**Concentration (mg mL^{-1})**	**Absorbance (280 nm)**
1	0.0001	0.1259
2	0.002	0.1592
5	0.005	0.2193
10	0.01	0.3333
12	0.012	0.3800

A graph of absorbance against concentration was plotted, using the formula y = mx + b, where y = absorbance of unknown substance, m = slope of graph of known concentration, x = concentration of unknown substance, b = intercept along y axis.

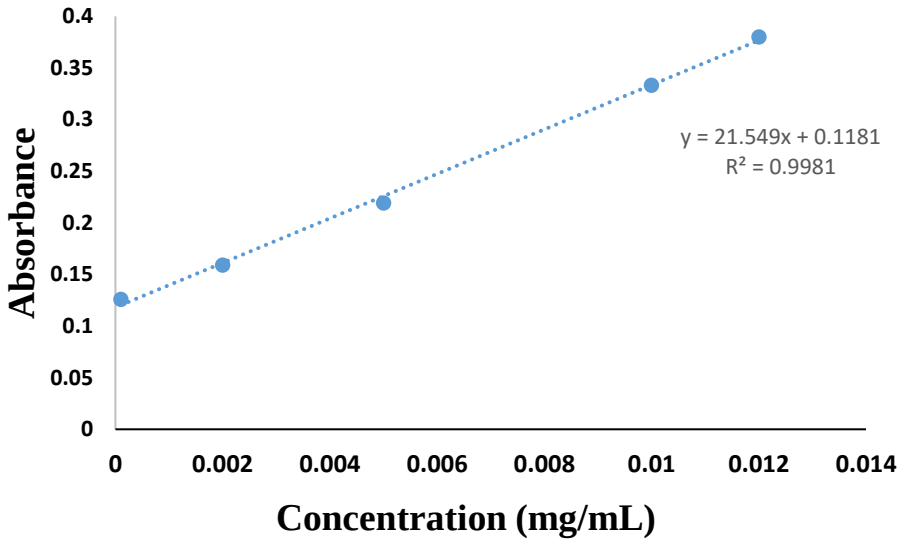

Figure 37. Calibration curve showing UV absorption of various concentration of FA.

Estimation of FA Concentration in FA-CDs

Using the formula above, the slope (m) of the graph is calculated to be **21.549**, while the intercept (b) on the y axis is **0.1181**. Absorbance of the unknown sample (FA-CDs), 0.1 mg mL^{-1} *(1mg/10mL)* of FA-CDs solution was prepared, absorbance was measured at 280 nm to be **0.876**, which is the fingerprint absorbance of FA.

Substituting into the formula **y = mx + b** and solving for x;

y = 0.8760 *(absorbance of unknown compound)*;

b = 0.1181 *(intercept);*

m = 21.549 *(slope)*

x *(concentration of the unknown)* = **0.03511 mg mL^{-1}**

FA used for preparation: 20 mg/(8+4+2)mL= 1.42 mg/mL

FA in FA-CDs: (1.42 mg/mL x 1 mL - 0.03511 mg/mL x1 mL)/1 mL= 1.3849 mg/mL

Estimation of In Vitro Drug Release

To investigate the release properties and load efficiency of FA-CDs-Dox, 3 mL of the resultant solution was dialyzed using a dialysis membrane (MWCO = 1,000 Da) against 120 mL PBS buffer solution at pH 7.4 for 72 hours. In some intervals, 1 mL of the release medium was taken and replaced with equal volume of PBS. A UV-vis spectroscopy of the sample was then taken at an absorbance of 485 nm, the concentration of the sample is then calculated using the standard calibration curve to determine the sample's concentration and amount of drug released.[88]

At different intervals of 1 hrs, 6 hrs, 18 hrs, 47 hrs, 51 hrs, 67 hrs and 72 hrs, 1 mL of the release medium was taken, and replaced with equal volume of the buffer solution and the absorbance measured, Table 5 below shows the result of the data obtained. The amount of drug in the released medium was determined using excel with the formula;

Amount of drug = Concentration (mg/mL) × Volume of medium (mL) × dilution factor.

% drug release (CDR) = amount of drug (mg) / theoretical drug amount (mg) × 100

Table 5. Showing Concentration of Different Samples and the Cumulative Drug Release (CDR)

Sr No.	Time (hrs.)	Abs (A)	Conc. (mg/ml)	Amt. (mg)	CDR (%)
1	1	0.008	0.00249	0.298	29.824
2	6	0.018	0.00294	0.353	35.278
3	18	0.036	0.00376	0.451	45.096
4	47	0.055	0.00462	0.555	55.459
5	51	0.061	0.00489	0.587	58.732
6	67	0.068	0.00521	0.626	62.550
7	72	0.077	0.00562	0.675	67.459

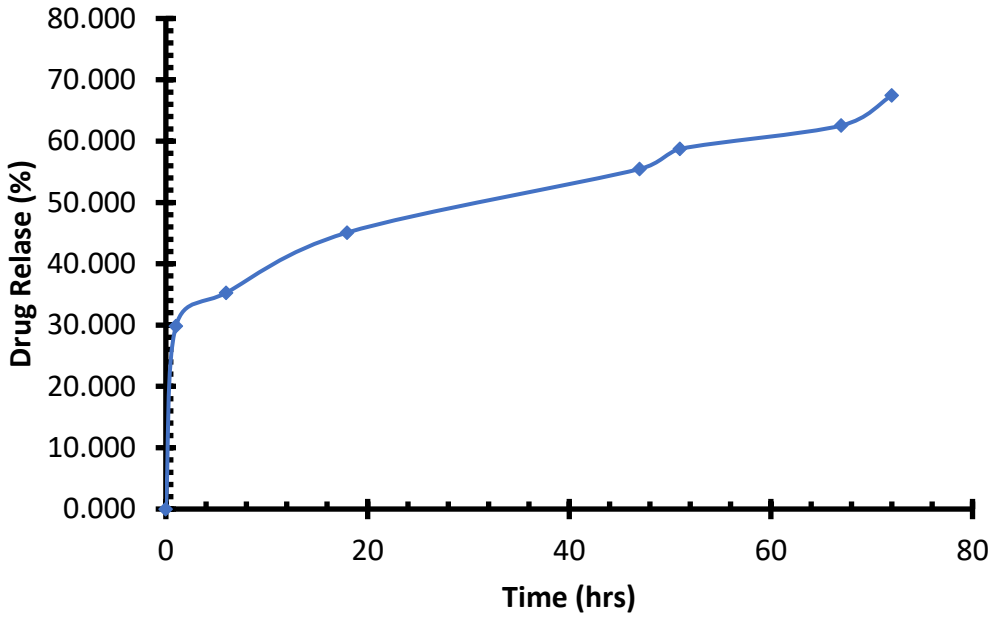

Figure 38. Graph showing the drug released in vitro at regular intervals at pH 7.4 PBS Buffer.

Determination of Dox Concentration in FA-CDs-Dox (from CDs sample B)

1 mL of FA-CDs solution (8 mg mL^{-1}) and 1 mL of Dox solution (1 mg mL^{-1}) were mixed with PBS at pH 7.4 under stirring to form a final solution system of 4 mL. This solution was then allowed to react for 48 hours at constant stirring on a sand bath set at 25 ^{o}C and 200 rpm in the dark to prevent photodegradation of Dox.

To investigate the release properties and load efficiency of FA-CDs-Dox, 3 mL of the resultant solution was dialyzed using a dialysis membrane (MWCO = 1,000 Da) against 120 mL PBS buffer solution at pH 7.4 for 72 hours. In some intervals, 1mL of the release medium was taken and replaced with equal volume of PBS. A UV-vis spectroscopy of the sample was then taken at an absorbance of 485 nm, the concentration of the sample is then calculated using the standard calibration curve to determine the sample's concentration and amount of drug released.

Calculation of Weight of the Unknown (W_f)

Since concentration (mg mL^{-1}) = mass/volume (mL)

Volume of FA-CDs-Dox after dialysis was 2.5 mL

0.0967 mg mL^{-1} = mass/ 2.5 mL

Mass (W_f) = **0.24175 mg**

DLC and DLE Calculation (Sample B)

Loading content (%) = $\frac{W_t - W_f}{W_{CD-FA}} \times 100$

Loading efficiency (%) = $\frac{W_t - W_f}{W_t} \times 100$

W_t = 1.00 mg; W_f = 0.242 mg; $W_{FA\text{-}CDs}$ = 8.00 mg

Hence,

DLC = 9.48 %; DLE = 75.8 %

Table 6. Drug Load Characteristics of FA-CDs-Dox (sample B)

Sample	Weight of FA-CDs (mg)	Weight of DOX (mg)	DLC (%)	DLE (%)
FA-CDs-Dox	8.0	1.0	9.48	75.8

Discussion on DLC and DLE

Using the technique described above, FA-CDs-Dox from sample B showed more drug load content (9.48%) compared to sample A (4.45%), this may be because 1.0 mg of Dox was loaded to the FA-CDs NP (prepared from sample B), while 0.4 mg of Dox was loaded on FA-CDs (prepared from sample A). Even though the amount of Dox used is higher in sample B than in sample A, the load efficiency is higher in sample A (89.1%) than in sample B (75.8%). Unsurprisingly, by increasing the weight of Dox used, it is possible to increase the drug load content of the samples but not necessarily the efficiency. Generally, both samples showed good load content and efficiency. This result also proves that it is possible to load Dox on the FA-CDs NP via electrostatic interaction.

CHAPTER 4. CONCLUSION AND FUTURE WORK

Two series of CDs, FA-CDs and FA-CDs-Dox, were successfully prepared in the lab and their physical properties was observed and compared. The optical properties of the all samples were examined using UV-vis, FL spectroscopy, and FTIR. The FA-CDs-Dox showed high load capacity, efficiency and drug release. It was also observed that changing the ratio of the precursor of CDs have little effect on the overall optical properties, the pharmaceutical test on the diagnostic and therapeutic anticancer potential of the NPs are still under investigation. However, CDs prepared from equal ratio of citric acid and ethylenediamine might be preferable to due ease of preparation, and better optical properties. The results showed that CDs based drug delivery vehicles can have effective application in cancer chemotherapy. Future studies will attempt to focus on changing the chemotherapeutic agent. The NP will be tested on different cancer cell lines to monitor its efficiency as well as effectiveness and if it is selective to cancer cell tumors. The *in vivo* studies of the NPs will also be examined as well as future clinical applications.

REFERENCES

(1) Prager, G. W.; Braga, S.; Bystricky, B.; Qvortrup, C.; Criscitiello, C.; Esin, E.; Sonke, G. S.; Martínez, G. A.; Frenel, J.-S.; Karamouzis, M.; et al. Global Cancer Control: Responding to the Growing Burden, Rising Costs and Inequalities in Access. *ESMO Open* **2018**, *3* (2), e000285. https://doi.org/10.1136/esmoopen-2017-000285.

(2) World Health Organization: International Agency for Research on Cancer. Latest Global Cancer Data (Released Sept 12, 2018).

(3) Mr, A. Breast Cancer and Associated Factors: A Review. **2015**, *8* (4), 6.

(4) Jemal, A.; Siegel, R.; Xu, J.; Ward, E. Cancer Statistics, 2010. *CA. Cancer J. Clin.* **2010**, *60* (5), 277–300. https://doi.org/10.3322/caac.20073.

(5) Meng, H.; Zink, J. I.; Donahue, T.; Radu, C.; Wainberg, Z.; Nel, A. Cancer Nanotechnology Plan 2015. **2015**, 257.

(6) National Cancer Institute. What Is Cancer? https://www.cancer.gov/about-cancer/understanding/what-is-cancer (Accessed August 12, 2019)

(7) Song, S.; Shen, H.; Yang, T.; Wang, L.; Fu, H.; Chen, H.; Zhang, Z. Indocyanine Green Loaded Magnetic Carbon Nanoparticles for Near Infrared Fluorescence/Magnetic Resonance Dual-Modal Imaging and Photothermal Therapy of Tumor. *ACS Appl. Mater. Interfaces* **2017**, *9* (11), 9484–9495. https://doi.org/10.1021/acsami.7b00490.

(8) Yuan, Y.; Guo, B.; Hao, L.; Liu, N.; Lin, Y.; Guo, W.; Li, X.; Gu, B. Doxorubicin-Loaded Environmentally Friendly Carbon Dots as a Novel Drug Delivery System for Nucleus Targeted Cancer Therapy. *Colloids Surf. B Biointerfaces* **2017**, *159*, 349–359. https://doi.org/10.1016/j.colsurfb.2017.07.030.

(9) Pageni, P. Synthesis of Ester Derivatives of Resveratrol as Potential Anti-Cancer Drugs. *Electron. Theses Diss.* **2013**, 67. https://dc.etsu.edu/etd/1181.

(10) Yang, L.; Wang, Z.; Wang, J.; Jiang, W.; Jiang, X.; Bai, Z.; He, Y.; Jiang, J.; Wang, D.; Yang, L. Doxorubicin Conjugated Functionalizable Carbon Dots for Nucleus Targeted Delivery and Enhanced Therapeutic Efficacy. *Nanoscale* **2016**, *8* (12), 6801–6809. https://doi.org/10.1039/C6NR00247A.

(11) Hira, S. K.; Mishra, A. K.; Ray, B.; Manna, P. P. Targeted Delivery of Doxorubicin-Loaded Poly (ε-Caprolactone)-b-Poly (N-Vinylpyrrolidone) Micelles Enhances Antitumor Effect in Lymphoma. *PLoS ONE* **2014**, *9* (4), e94309. https://doi.org/10.1371/journal.pone.0094309.

(12) Gulati, Y. *How to Remember Classification of Anticancer Drugs - Pharmacology Made Simple*; 2018.

(13) Bhunia, S. K.; Saha, A.; Maity, A. R.; Ray, S. C.; Jana, N. R. Carbon Nanoparticle-Based Fluorescent Bioimaging Probes. *Sci. Rep.* **2013**, *3*. https://doi.org/10.1038/srep01473.

(14) Pardo, J.; Peng, Z.; Leblanc, R. Cancer Targeting and Drug Delivery Using Carbon-Based Quantum Dots and Nanotubes. *Molecules* **2018**, *23* (2), 378. https://doi.org/10.3390/molecules23020378.

(15) Sun, Y.-P.; Zhou, B.; Lin, Y.; Wang, W.; Fernando, K. S.; Pathak, P.; Meziani, M. J.; Harruff, B. A.; Wang, X.; Wang, H. Quantum-Sized Carbon Dots for Bright and Colorful Photoluminescence. *J. Am. Chem. Soc.* **2006**, *128* (24), 7756–7757.

(16) Tao, H.; Yang, K.; Ma, Z.; Wan, J.; Zhang, Y.; Kang, Z.; Liu, Z. In Vivo NIR Fluorescence Imaging, Biodistribution, and Toxicology of Photoluminescent Carbon Dots

Produced from Carbon Nanotubes and Graphite. *Small* **2012**, *8* (2), 281–290. https://doi.org/10.1002/smll.201101706.

(17) Patel, K. D.; Singh, R. K.; Kim, H.-W. Carbon-Based Nanomaterials as an Emerging Platform for Theranostics. *Mater. Horiz.* **2019**, *6* (3), 434–469. https://doi.org/10.1039/C8MH00966J.

(18) Bruchez Jr., M. Semiconductor Nanocrystals as Fluorescent Biological Labels. *Science* **1998**, *281* (5385), 2013–2016. https://doi.org/10.1126/science.281.5385.2013.

(19) Murray, C. B.; Norris, D. J.; Bawendi, M. G. Synthesis and Characterization of Nearly Monodisperse CdE (E = Sulfur, Selenium, Tellurium) Semiconductor Nanocrystallites. *J. Am. Chem. Soc.* **1993**, *115* (19), 8706–8715. https://doi.org/10.1021/ja00072a025.

(20) Hines, M. A.; Guyot-Sionnest, P. Synthesis and Characterization of Strongly Luminescing ZnS-Capped CdSe Nanocrystals. *J. Phys. Chem.* **1996**, *100* (2), 468–471. https://doi.org/10.1021/jp9530562.

(21) Hines, M. A.; Guyot-Sionnest, P. Bright UV-Blue Luminescent Colloidal ZnSe Nanocrystals. *J. Phys. Chem. B* **1998**, *102* (19), 3655–3657. https://doi.org/10.1021/jp9810217.

(22) Peng, Z. A.; Peng, X. Formation of High-Quality CdTe, CdSe, and CdS Nanocrystals Using CdO as Precursor. *J. Am. Chem. Soc.* **2001**, *123* (1), 183–184. https://doi.org/10.1021/ja003633m.

(23) Drbohlavova, J.; Adam, V.; Kizek, R.; Hubalek, J. Quantum Dots — Characterization, Preparation and Usage in Biological Systems. *Int. J. Mol. Sci.* **2009**, *10* (2), 656–673. https://doi.org/10.3390/ijms10020656.

(24) Deerinck, T. J. The Application of Fluorescent Quantum Dots to Confocal, Multiphoton, and Electron Microscopic Imaging. *Toxicol. Pathol.* **2008**, *36* (1), 112–116. https://doi.org/10.1177/0192623307310950.

(25) Michalet, X. Quantum Dots for Live Cells, in Vivo Imaging, and Diagnostics. *Science* **2005**, *307* (5709), 538–544. https://doi.org/10.1126/science.1104274.

(26) Walling, M.; Novak, J.; Shepard, J. R. E. Quantum Dots for Live Cell and In Vivo Imaging. *Int. J. Mol. Sci.* **2009**, *10* (2), 441–491. https://doi.org/10.3390/ijms10020441.

(27) Chan, W. C. Quantum Dot Bioconjugates for Ultrasensitive Nonisotopic Detection. *Science* **1998**, *281* (5385), 2016–2018. https://doi.org/10.1126/science.281.5385.2016.

(28) Lin, S.; Xie, X.; Patel, M. R.; Yang, Y.-H.; Li, Z.; Cao, F.; Gheysens, O.; Zhang, Y.; Gambhir, S. S.; Rao, J.; et al. Quantum Dot Imaging for Embryonic Stem Cells. *BMC Biotechnol.* **2007**, *7* (1), 67. https://doi.org/10.1186/1472-6750-7-67.

(29) Molaei, M. J. Carbon Quantum Dots and Their Biomedical and Therapeutic Applications: A Review. *RSC Adv.* **2019**, *9* (12), 6460–6481. https://doi.org/10.1039/C8RA08088G.

(30) Peng, Z.; Han, X.; Li, S.; Al-Youbi, A. O.; Bashammakh, A. S.; El-Shahawi, M. S.; Leblanc, R. M. Carbon Dots: Biomacromolecule Interaction, Bioimaging and Nanomedicine. *Coord. Chem. Rev.* **2017**, *343*, 256–277. https://doi.org/10.1016/j.ccr.2017.06.001.

(31) Zhu, S.; Meng, Q.; Wang, L.; Zhang, J.; Song, Y.; Jin, H.; Zhang, K.; Sun, H.; Wang, H.; Yang, B. Highly Photoluminescent Carbon Dots for Multicolor Patterning, Sensors, and Bioimaging. *Angew. Chem.* **2013**, *125* (14), 4045–4049.

(32) Gan, Z.; Hao, Y.; Shan, Y. Temperature-Dependent Dual Emission from Sucrose-Derived Carbon Nanodots: A Ratiometric Fluorescent Thermometer. *ChemNanoMat* **2016**, *2* (3), 171–175. https://doi.org/10.1002/cnma.201500228.

(33) Cao, L.; Wang, X.; Meziani, M. J.; Lu, F.; Wang, H.; Luo, P. G.; Lin, Y.; Harruff, B. A.; Veca, L. M.; Murray, D. Carbon Dots for Multiphoton Bioimaging. *J. Am. Chem. Soc.* **2007**, *129* (37), 11318–11319.

(34) Li, X.; Wang, H.; Shimizu, Y.; Pyatenko, A.; Kawaguchi, K.; Koshizaki, N. Preparation of Carbon Quantum Dots with Tunable Photoluminescence by Rapid Laser Passivation in Ordinary Organic Solvents. *Chem Commun* **2011**, *47* (3), 932–934. https://doi.org/10.1039/C0CC03552A.

(35) Dong, Y.; Pang, H.; Yang, H. B.; Guo, C.; Shao, J.; Chi, Y.; Li, C. M.; Yu, T. Carbon-Based Dots Co-Doped with Nitrogen and Sulfur for High Quantum Yield and Excitation-Independent Emission. *Angew. Chem. Int. Ed.* **2013**, *52* (30), 7800–7804. https://doi.org/10.1002/anie.201301114.

(36) Wang, X.; Qu, K.; Xu, B.; Ren, J.; Qu, X. Microwave Assisted One-Step Green Synthesis of Cell-Permeable Multicolor Photoluminescent Carbon Dots without Surface Passivation Reagents. *J. Mater. Chem.* **2011**, *21* (8), 2445. https://doi.org/10.1039/c0jm02963g.

(37) Zhu, H.; Wang, X.; Li, Y.; Wang, Z.; Yang, F.; Yang, X. Microwave Synthesis of Fluorescent Carbon Nanoparticles with Electrochemiluminescence Properties. *Chem. Commun.* **2009**, No. 34, 5118. https://doi.org/10.1039/b907612c.

(38) Liu, R.; Wu, D.; Liu, S.; Koynov, K.; Knoll, W.; Li, Q. An Aqueous Route to Multicolor Photoluminescent Carbon Dots Using Silica Spheres as Carriers. *Angew. Chem.* **2009**, *121* (25), 4668–4671.

(39) Wang, Y.; Hu, A. Carbon Quantum Dots: Synthesis, Properties and Applications. *J. Mater. Chem. C* **2014**, *2* (34), 6921. https://doi.org/10.1039/C4TC00988F.

(40) Yang, S.-T.; Cao, L.; Luo, P. G.; Lu, F.; Wang, X.; Wang, H.; Meziani, M. J.; Liu, Y.; Qi, G.; Sun, Y.-P. Carbon Dots for Optical Imaging in Vivo. *J. Am. Chem. Soc.* **2009**, *131* (32), 11308–11309.

(41) Li, S.; Peng, Z.; Dallman, J.; Baker, J.; Othman, A. M.; Blackwelder, P. L.; Leblanc, R. M. Crossing the Blood–Brain–Barrier with Transferrin Conjugated Carbon Dots: A Zebrafish Model Study. *Colloids Surf. B Biointerfaces* **2016**, *145*, 251–256. https://doi.org/10.1016/j.colsurfb.2016.05.007.

(42) Li, S.; Skromne, I.; Peng, Z.; Dallman, J.; Al-Youbi, A. O.; Bashammakh, A. S.; El-Shahawi, M. S.; Leblanc, R. M. "Dark" Carbon Dots Specifically "Light-up" Calcified Zebrafish Bones. *J. Mater. Chem. B* **2016**, *4* (46), 7398–7405. https://doi.org/10.1039/C6TB02241C.

(43) Yang, L.; Wang, Z.; Wang, J.; Jiang, W.; Jiang, X.; Bai, Z.; He, Y.; Jiang, J.; Wang, D.; Yang, L. Doxorubicin Conjugated Functionalizable Carbon Dots for Nucleus Targeted Delivery and Enhanced Therapeutic Efficacy. 10.

(44) Thakur, M.; Kumawat, M. K.; Srivastava, R. Multifunctional Graphene Quantum Dots for Combined Photothermal and Photodynamic Therapy Coupled with Cancer Cell Tracking Applications. *RSC Adv.* **2017**, *7* (9), 5251–5261. https://doi.org/10.1039/C6RA25976F.

(45) Lv, S.; Wu, Y.; Cai, K.; He, H.; Li, Y.; Lan, M.; Chen, X.; Cheng, J.; Yin, L. High Drug Loading and Sub-Quantitative Loading Efficiency of Polymeric Micelles Driven by Donor–Receptor Coordination Interactions. *J. Am. Chem. Soc.* **2018**, *140* (4), 1235–1238. https://doi.org/10.1021/jacs.7b12776.

(46) Luo, P. G.; Sahu, S.; Yang, S.-T.; Sonkar, S. K.; Wang, J.; Wang, H.; LeCroy, G. E.; Cao, L.; Sun, Y.-P. Carbon "Quantum" Dots for Optical Bioimaging. *J. Mater. Chem. B* **2013**, *1* (16), 2116–2127.

(47) Leménager, G.; De Luca, E.; Sun, Y.-P.; Pompa, P. P. Super-Resolution Fluorescence Imaging of Biocompatible Carbon Dots. *Nanoscale* **2014**, *6* (15), 8617. https://doi.org/10.1039/C4NR01970A.

(48) Song, Y.; Zhu, S.; Yang, B. Bioimaging Based on Fluorescent Carbon Dots. *RSC Adv.* **2014**, *4* (52), 27184. https://doi.org/10.1039/c3ra47994c.

(49) Wang, F. White Light-Emitting Devices Based on Carbon Dots' Electroluminescencew. **2011**, 3.

(50) Li, H.; He, X.; Kang, Z.; Huang, H.; Liu, Y.; Liu, J.; Lian, S.; Tsang, C. H. A.; Yang, X.; Lee, S.-T. Water-Soluble Fluorescent Carbon Quantum Dots and Photocatalyst Design. *Angew. Chem. Int. Ed.* **2010**, *49* (26), 4430–4434. https://doi.org/10.1002/anie.200906154.

(51) Cao, L.; Sahu, S.; Anilkumar, P.; Bunker, C. E.; Xu, J.; Fernando, K. A. S.; Wang, P.; Guliants, E. A.; Tackett, K. N.; Sun, Y.-P. Carbon Nanoparticles as Visible-Light Photocatalysts for Efficient CO_2 Conversion and Beyond. *J. Am. Chem. Soc.* **2011**, *133* (13), 4754–4757. https://doi.org/10.1021/ja200804h.

(52) Fernando, K. A. S.; Sahu, S.; Liu, Y.; Lewis, W. K.; Guliants, E. A.; Jafariyan, A.; Wang, P.; Bunker, C. E.; Sun, Y.-P. Carbon Quantum Dots and Applications in Photocatalytic Energy Conversion. *ACS Appl. Mater. Interfaces* **2015**, *7* (16), 8363–8376. https://doi.org/10.1021/acsami.5b00448.

(53) Zhao, T.; Zhang, S.; Guo, Y.; Wang, Q. TiC_2 : A New Two-Dimensional Sheet beyond MXenes. *Nanoscale* **2016**, *8* (1), 233–242. https://doi.org/10.1039/C5NR04472C.

(54) Boakye-Yiadom, K. O.; Kesse, S.; Opoku-Damoah, Y.; Filli, M. S.; Aquib, M.; Joelle, M. M. B.; Farooq, M. A.; Mavlyanova, R.; Raza, F.; Bavi, R.; et al. Carbon Dots: Applications in Bioimaging and Theranostics. *Int. J. Pharm.* **2019**, *564*, 308–317. https://doi.org/10.1016/j.ijpharm.2019.04.055.

(55) Kasouni, A.; Chatzimitakos, T.; Stalikas, C. Bioimaging Applications of Carbon Nanodots: A Review. *C* **2019**, *5* (2), 19. https://doi.org/10.3390/c5020019.

(56) Nie, S. Understanding and Overcoming Major Barriers in Cancer Nanomedicine. *Nanomed.* **2010**, *5* (4), 523–528. https://doi.org/10.2217/nnm.10.23.

(57) Liu, C.; Zhang, P.; Zhai, X.; Tian, F.; Li, W.; Yang, J.; Liu, Y.; Wang, H.; Wang, W.; Liu, W. Nano-Carrier for Gene Delivery and Bioimaging Based on Carbon Dots with PEI-Passivation Enhanced Fluorescence. *Biomaterials* **2012**, *33* (13), 3604–3613. https://doi.org/10.1016/j.biomaterials.2012.01.052.

(58) Tuerhong, M.; Xu, Y.; Yin, X.-B. Review on Carbon Dots and Their Applications. *Chin. J. Anal. Chem.* **2017**, *45* (1), 139–150. https://doi.org/10.1016/S1872-2040(16)60990-8.

(59) Lai, C.-W.; Hsiao, Y.-H.; Peng, Y.-K.; Chou, P.-T. Facile Synthesis of Highly Emissive Carbon Dots from Pyrolysis of Glycerol; Gram Scale Production of Carbon Dots/MSiO2 for Cell Imaging and Drug Release. *J. Mater. Chem.* **2012**, *22* (29), 14403. https://doi.org/10.1039/c2jm32206d.

(60) Sun, X.; Lei, Y. Fluorescent Carbon Dots and Their Sensing Applications. *TrAC Trends Anal. Chem.* **2017**, *89*, 163–180. https://doi.org/10.1016/j.trac.2017.02.001.

(61) Lu, W.; Qin, X.; Liu, S.; Chang, G.; Zhang, Y.; Luo, Y.; Asiri, A. M.; Al-Youbi, A. O.; Sun, X. Economical, Green Synthesis of Fluorescent Carbon Nanoparticles and Their Use

as Probes for Sensitive and Selective Detection of Mercury(II) Ions. *Anal. Chem.* **2012**, *84* (12), 5351–5357. https://doi.org/10.1021/ac3007939.

(62) Wei, X.-M.; Xu, Y.; Li, Y.-H.; Yin, X.-B.; He, X.-W. Ultrafast Synthesis of Nitrogen-Doped Carbon Dots via Neutralization Heat for Bioimaging and Sensing Applications. *RSC Adv* **2014**, *4* (84), 44504–44508. https://doi.org/10.1039/C4RA08523J.

(63) Zhu, S.; Meng, Q.; Wang, L.; Zhang, J.; Song, Y.; Jin, H.; Zhang, K.; Sun, H.; Wang, H.; Yang, B. Highly Photoluminescent Carbon Dots for Multicolor Patterning, Sensors, and Bioimaging. *Angew. Chem. Int. Ed.* **2013**, *52* (14), 3953–3957. https://doi.org/10.1002/anie.201300519.

(64) Assaraf, Y. G.; Leamon, C. P.; Reddy, J. A. The Folate Receptor as a Rational Therapeutic Target for Personalized Cancer Treatment. *Drug Resist. Updat.* **2014**, *17* (4–6), 89–95. https://doi.org/10.1016/j.drup.2014.10.002.

(65) O'Shannessy, D. J.; Yu, G.; Smale, R.; Fu, Y.-S.; Singhal, S.; Thiel, R. P.; Somers, E. B.; Vachani, A. Folate Receptor Alpha Expression in Lung Cancer: Diagnostic and Prognostic Significance. *Oncotarget* **2012**, *3* (4). https://doi.org/10.18632/oncotarget.519.

(66) Yoo, H. S.; Park, T. G. Folate-Receptor-Targeted Delivery of Doxorubicin Nano-Aggregates Stabilized by Doxorubicin–PEG–Folate Conjugate. *J. Controlled Release* **2004**, *100* (2), 247–256. https://doi.org/10.1016/j.jconrel.2004.08.017.

(67) Zhao, X.; Zhang, J.; Shi, L.; Xian, M.; Dong, C.; Shuang, S. Folic Acid-Conjugated Carbon Dots as Green Fluorescent Probes Based on Cellular Targeting Imaging for Recognizing Cancer Cells. *RSC Adv.* **2017**, *7* (67), 42159–42167. https://doi.org/10.1039/C7RA07002K.

(68) Zwicke, G. L.; Ali Mansoori, G.; Jeffery, C. J. Utilizing the Folate Receptor for Active Targeting of Cancer Nanotherapeutics. *Nano Rev.* **2012**, *3* (1), 18496. https://doi.org/10.3402/nano.v3i0.18496.

(69) Mewada, A.; Pandey, S.; Thakur, M.; Jadhav, D.; Sharon, M. Swarming Carbon Dots for Folic Acid Mediated Delivery of Doxorubicin and Biological Imaging. *J Mater Chem B* **2014**, *2* (6), 698–705. https://doi.org/10.1039/C3TB21436B.

(70) Zhang, X.; Meng, L.; Lu, Q.; Fei, Z.; Dyson, P. J. Targeted Delivery and Controlled Release of Doxorubicin to Cancer Cells Using Modified Single Wall Carbon Nanotubes. *Biomaterials* **2009**, *30* (30), 6041–6047. https://doi.org/10.1016/j.biomaterials.2009.07.025.

(71) Huang, H.; Yuan, Q.; Shah, J. S.; Misra, R. D. K. A New Family of Folate-Decorated and Carbon Nanotube-Mediated Drug Delivery System: Synthesis and Drug Delivery Response. *Adv. Drug Deliv. Rev.* **2011**, *63* (14–15), 1332–1339. https://doi.org/10.1016/j.addr.2011.04.001.

(72) Yin, M.; Wang, M.; Miao, F.; Ji, Y.; Tian, Z.; Shen, H.; Jia, N. Water-Dispersible Multiwalled Carbon Nanotube/Iron Oxide Hybrids as Contrast Agents for Cellular Magnetic Resonance Imaging. *Carbon* **2012**, *50* (6), 2162–2170. https://doi.org/10.1016/j.carbon.2012.01.026.

(73) Low, P. S.; Henne, W. A.; Doorneweerd, D. D. Discovery and Development of Folic-Acid-Based Receptor Targeting for Imaging and Therapy of Cancer and Inflammatory Diseases. *Acc. Chem. Res.* **2008**, *41* (1), 120–129. https://doi.org/10.1021/ar7000815.

(74) Muller, C.; Schibli, R. Folic Acid Conjugates for Nuclear Imaging of Folate Receptor-Positive Cancer. *J. Nucl. Med.* **2011**, *52* (1), 1–4. https://doi.org/10.2967/jnumed.110.076018.

(75) Schwingshackl, L.; Boeing, H.; Stelmach-Mardas, M.; Gottschald, M.; Dietrich, S.; Hoffmann, G.; Chaimani, A. Dietary Supplements and Risk of Cause-Specific Death, Cardiovascular Disease, and Cancer: A Systematic Review and Meta-Analysis of Primary Prevention Trials. *Adv. Nutr. Int. Rev. J.* **2017**, *8* (1), 27–39. https://doi.org/10.3945/an.116.013516.

(76) Rivankar, S. An Overview of Doxorubicin Formulations in Cancer Therapy. *J. Cancer Res. Ther.* **2014**, *10* (4), 853. https://doi.org/10.4103/0973-1482.139267.

(77) Gamen, S.; Anel, A.; Pérez-Galán, P.; Lasierra, P.; Johnson, D.; Piñeiro, A.; Naval, J. Doxorubicin Treatment Activates a Z-VAD-Sensitive Caspase, Which Causes ΔΨm Loss, Caspase-9 Activity, and Apoptosis in Jurkat Cells. *Exp. Cell Res.* **2000**, *258* (1), 223–235. https://doi.org/10.1006/excr.2000.4924.

(78) Lorenzo, E.; Ruiz-Ruiz, C.; Quesada, A. J.; Hernández, G.; Rodríguez, A.; López-Rivas, A.; Redondo, J. M. Doxorubicin Induces Apoptosis and *CD95* Gene Expression in Human Primary Endothelial Cells through a P53-Dependent Mechanism. *J. Biol. Chem.* **2002**, *277* (13), 10883–10892. https://doi.org/10.1074/jbc.M107442200.

(79) Takemura, G.; Fujiwara, H. Doxorubicin-Induced Cardiomyopathy. *Prog. Cardiovasc. Dis.* **2007**, *49* (5), 330–352. https://doi.org/10.1016/j.pcad.2006.10.002.

(80) Meng, F.; Zhong, Y.; Cheng, R.; Deng, C.; Zhong, Z. PH-Sensitive Polymeric Nanoparticles for Tumor-Targeting Doxorubicin Delivery: Concept and Recent Advances. *Nanomed.* **2014**, *9* (3), 487–499. https://doi.org/10.2217/nnm.13.212.

(81) Lee, H. U.; Park, S. Y.; Park, E. S.; Son, B.; Lee, S. C.; Lee, J. W.; Lee, Y.-C.; Kang, K. S.; Kim, M. I.; Park, H. G.; et al. Photoluminescent Carbon Nanotags from Harmful Cyanobacteria for Drug Delivery and Imaging in Cancer Cells. *Sci. Rep.* **2015**, *4* (1), 4665. https://doi.org/10.1038/srep04665.

(82) Li, S.; Amat, D.; Peng, Z.; Vanni, S.; Raskin, S.; De Angulo, G.; Othman, A. M.; Graham, R. M.; Leblanc, R. M. Transferrin Conjugated Nontoxic Carbon Dots for Doxorubicin Delivery to Target Pediatric Brain Tumor Cells. *Nanoscale* **2016**, *8* (37), 16662–16669. https://doi.org/10.1039/C6NR05055G.

(83) Jung, Y. K.; Shin, E.; Kim, B.-S. Cell Nucleus-Targeting Zwitterionic Carbon Dots. *Sci. Rep.* **2015**, *5* (1). https://doi.org/10.1038/srep18807.

(84) Penner, M. H. Ultraviolet, Visible, and Fluorescence Spectroscopy. In *Food Analysis*; Nielsen, S. S., Ed.; Springer US: Boston, MA, 2010; pp 387–405. https://doi.org/10.1007/978-1-4419-1478-1_22.

(85) Penner, M. H. Basic Principles of Spectroscopy. In *Food Analysis*; Nielsen, S. S., Ed.; Springer US: Boston, MA, 2010; pp 375–385. https://doi.org/10.1007/978-1-4419-1478-1_21.

(86) Fong, J. F. Y. Development of Biocompatible Carbon Nanoparticles for Optical Sensing Applications. 274.

(87) *Principles of Fluorescence Spectroscopy*; Lakowicz, J. R., Ed.; Springer US: Boston, MA, 2006. https://doi.org/10.1007/978-0-387-46312-4.

(88) Kong, T.; Hao, L.; Wei, Y.; Cai, X.; Zhu, B. Doxorubicin Conjugated Carbon Dots as a Drug Delivery System for Human Breast Cancer Therapy. *Cell Prolif.* **2018**, *51* (5), e12488. https://doi.org/10.1111/cpr.12488.

(89) O'Haver, T. Comparison of Calibration Curve Fitting Methods in Absorption Spectroscopy. May 17, 2008.

(90) Zhang, Z.; Lei, Y.; Yang, X.; Shi, N.; Geng, L.; Wang, S.; Zhang, J.; Shi, S. High Drug-Loading System of Hollow Carbon Dots–Doxorubicin: Preparation, *in Vitro* Release and PH-Targeted Research. *J. Mater. Chem. B* **2019**, *7* (13), 2130–2137. https://doi.org/10.1039/C9TB00032A.

(91) Dada, S. N.; Hua, M. Preparation of Folic Acid-Carbon Dots-Doxorubicin Nanoparticles as Targeting Tumor Theranostics.

(92) Mohammad, F.; Bwatanglang, I. birma; Yusof, N. A.; Abdullah, J.; Hussein, M. Z.; Alitheen, N. B.; Abu, N. Folic Acid Targeted Mn:ZnS Quantum Dots for Theranostic Applications of Cancer Cell Imaging and Therapy. *Int. J. Nanomedicine* **2016**, 413. https://doi.org/10.2147/IJN.S90198.

(93) Sureshkumar, S.; Jothimani, B.; Sridhar, T. M.; Santhosh, A.; Venkatachalapathy, B. Synthesis of Hexagonal ZnO-PQ7 Nano Disks Conjugated with Folic Acid to Image MCF – 7 Cancer Cells. *J. Fluoresc.* **2017**, *27* (1), 21–29. https://doi.org/10.1007/s10895-016-1932-y.

(94) Liang, J.; Zhang, Z.; Zhao, H.; Wan, S.; Zhai, X.; Zhou, J.; Liang, R.; Deng, Q.; Wu, Y.; Lin, G. Simple and Rapid Monitoring of Doxorubicin Using Streptavidin-Modified Microparticle-Based Time-Resolved Fluorescence Immunoassay. *RSC Adv.* **2018**, *8* (28), 15621–15631. https://doi.org/10.1039/C8RA01807C.

VITA

SAMSON DADA

Education:	B.Sc. Chemistry, Lagos State University, Ojo City, Lagos 2014 M.Sc. Chemistry, East Tennessee State University, Johnson City, Tennessee 2019
Professional Experience:	Business Support, BetaPlus Int'l Synergy Limited, Ikoyi, Lagos, 2016 – 2018 Graduate Assistant, East Tennessee State University, College of Arts and Sciences, 2018 – 2019
Publications:	Ogbu, C. I.; Feng, X.; Dada, S. N.; Bishop, G. W. Screen-Printed Soft-Nitrided Carbon Electrodes for Detection of Hydrogen Peroxide. Sensors 2019, 19 (17), 3741. Dada, S. N.; Hua, M. Preparation of Folic Acid-Carbon Dots-Doxorubicin Nanoparticles as Targeting Tumor Theranostics. *(manuscript in preparation)*.
Honors and Awards:	Outstanding Graduate Student, Department of Chemistry. Johnson City, East Tennessee State University. Office of Equity & Inclusion graduate Travel Grants Student, East Tennessee State University. 2019 Appalachian Student Research Forum Award First Place, Graduate Student-Master's Chemical Sciences, Poster Presentation, East Tennessee State University. Eastman-NETSACS student research poster symposium Award First runner-up, , Graduate Student, Poster Presentation, East Tennessee State University.